Discharge prediction in partly vegetated channel flows: Adaptation of IDCM method with a curved interface and large-scale roughness elements

Discharge prediction in partly vegetated channel flows: Adaptation of IDCM method with a curved interface and large-scale roughness elements

Mouldi Ben Meftah[1]*, Michele Mossa[1]

[1]Department of Civil, Environmental, Building Engineering and Chemistry, Polytechnic University of Bari, Via E. Orabona 4, 70125 Bari, Italy, e-mail: mouldi.benmeftah@poliba.it, michele.mossa@poliba.it

* Corresponding author: ph.: +39 080 5963508, fax: +39 080 5963414, e-mail: mouldi.benmeftah@poliba.it;

Abstract: This study provides new insight into how to predict flow discharges of partly vegetated channels with emergent vegetation. By adapting for the first time the Interacting Divided Channel Method (IDCM), applied with a curved interface approach and with the presence of large-scale roughness elements (not considered in previous studies), the total and zonal discharges of partly vegetated channels were predicted based on a series of experimental results in this study together with collected data from previous studies. Consideration of transverse momentum transfer in terms of apparent shear stress at curved interface plane showed better performance with IDCM than the Divided Channel Method (DCM) with both curved and classic vertical/diagonal divisions. In this study, we also proposed a series of expressions, easily applicable, to predict the zonal discharges of a partly vegetated channel.

Many experiments were carried out in a physical model of a very large rectangular channel with the presence of rows of vertical, rigid, circular, and rough steel cylinders, representing emergent rigid vegetation. The rows of cylinders were partially mounted on the bottom of the channel, leaving lateral areas of free circulation near the walls. The three-dimensional components of the flow velocity were measured using a 3D Acoustic Doppler Velocimeter (ADV)-Vectrino.

Keywords: partly vegetated channels, discharge prediction, apparent shear stress, IDCM method, curved interface, velocity measurements.

1. Introduction

Predicting flow discharge through river channels is significant for the design and operation of hydraulic structures, river restoration, and sustainable development planning (Huthoff et al., 2008; Al-Khatib et al., 2012; Yang et al., 2019). Currently, the world is facing the challenge of climate change which contributes to increasing the intensity and frequency of floods. Accurate estimation of flow conveyance in natural watercourses can help reduce the impact of floods on human life and property. In nature, many watercourses are composite compound channels, consisting of different subareas of varying geometry and roughness. Channels with fringing vegetation are found in many important environmental settings (White and Nepf, 2008). Partly vegetated channels show similar hydrodynamic behaviors as a compound channel, consisting of a main channel and one or two-side floodplains of varying geometry and roughness (Tang, 2017; Yang et al., 2019; Pradhan and Khatua, 2020). At the interface between the main channel and an adjacent vegetated area, a shear layer takes place. The large velocity gradient that occurs at the interface generates high turbulence and transverse momentum transfer from faster to slower flow subareas, reducing the velocity in the main channel and increasing it in the obstructed area. The variation in flow structures between different subsections increases the difficulty in accurately estimating flow discharge in composite/compound channels. The familiar methods often used to determine the flow conveyance for river channels are the Single Channel Method (SCM) and Divided Channel Method (DCM). Both methods are based on standard Chezy, Manning, and Darcy-Weisbach equations, treating the cross-section as a single channel or dividing it horizontally,

vertically, or diagonally into noninteracting subareas (Huthoff et al., 2008; Tang, 2017; Pradhan and Khatua, 2020).

Several workers have experimentally and numerically studied the flow in composite vegetated channels. White and Nepf (2008), summarizing different models and approaches to describe and predict flow features at the interface of partly vegetated channels, indicated that most models have used simplified one-dimensional approaches with an empirical Darcy-Weisbach friction factor or a simple eddy viscosity model for the turbulence structure. Based on the double averaged of Navier-Stokes equations, neglection the effect of vertical velocity component, White and Nepf (2008), Chen et al. (2010), Ben Meftah et al. (2014), Lima and Izumi (2014) and Ben Meftah and Mossa (2016), Li et al. (2022), as an example, proposed analytical solutions to predict the typical transversal profile of the mean flow velocity at the interface between the vegetated and non-vegetated areas. Despite the difficult application, these solutions can be used to predict the flow discharge in partly vegetated channels.

In previous studies (e.g., Prinos and Townsend, 1984; Al-Khatib et al., 2012; Parsaie et al., 2016), it was confirmed that conventional SCM and DCM methods overestimate or underestimate flow discharge. The SCM is known to underestimate the discharge capacity of compound channels, while DCM overestimates it (Myers and Brennan,1990; Pradhan and Khatua, 2020). In general, the DCM predicts better results as compared to SCM and it is currently used, because of its simplicity, for most practical models for open channel flows, i.e., HEC-RAS, SOBEK, MIKE 11 (Farooq et al., 2016; Tang, 2017). The classical divided channel method (DCM) without consideration of the interfacial effect, due to lateral momentum transfer, between the different subsections usually overestimates and underestimates the discharge in the main channel and floodplains, respectively (Singh and Tang, 2020).

Several approaches are proposed in the literature to improve the reliability of conveyance capacity prediction in compound channels. Huthoff et al. (2008) and Singh and Tang (2020) have well summarized most of these advanced approaches, classifying them into three classes:

i) ignorance of momentum transfer while shifting the position and shape of the interfaces which modifies the wetted area and perimeter in the Manning equations,

ii) introduction of interfacial apparent shear stress based on the secondary current and Reynolds stresses distribution due to flow velocity fluctuation. The interfacial apparent shear stress is usually parametrized in terms of the difference between main channel and floodplain velocities,

iii) continuum models based on solving the depth integrated and time-averaged Reynolds Averaged Navier-Stokes (RANS) equations or shallow water equations. This method is considered impractical because transverse numerical integration of the depth-averaged of the streamwise velocity is required to obtain a stage-discharge relationship.

In addition to the abovementioned three classes of methods, in literature, there are many other approaches (e.g., Ackers, 1993, Parsaie et al., 2016; Tang, 2017; Farhadi et al., 2019; Pradhan and Khatua, 2020) proposed to estimate the zonal and overall discharge in compound channels.

The large velocity gradient occurring at the interface between the main channel and the floodplain generates high turbulence and transverse momentum transfer from the fastest to the slowest flow area, reducing velocity in the main channel and increasing it in the floodplains. The momentum transfer mechanism, due to the formation of vortex structures at the interface between subsections, was experimentally discovered for the first time by Sellin (1964). Since this discovery, several studies (e.g., Myers, 1978; Knight and Demetriou, 1983; Huthoff et al., 2008; Tang, 2019; Pradhan and Khatua, 2020) have focused on considering the contribution of momentum transfer in terms of apparent shear stress for estimating flow discharge. It was concluded that interface momentum transfer accounting better predicts zonal and overall flow discharges in compound channels.

Most of the previous studies, which predict flow discharge, dealt with compound channels of similar or different bottom roughness in both the main channel and the floodplain compartments. Natural compound channels commonly consist of a main channel and floodplains covered with

vegetation. Aquatic vegetation has different properties (height, shape, roughness, bending stiffness, density) and can occupy the whole or part of a section of a watercourse (Ben Meftah and Mossa, 2016). In addition to the ecological functions, the presence of vegetation adjacent to watercourses also increases the flow resistance and affects the conveyance capacity (Hamidifar et al., 2016). Despite the several studies conducted on vegetated channels (Naot et al., 1996; Nepf, 1999; Ghisalberti and Nepf, 2004; White and Nepf, 2007; Ghisalberti, 2010; Cheng and Nguyen, 2011; Ben Meftah and Mossa, 2013; Ben Meftah et al., 2015; Liu and Zeng, 2017; Mossa et al., 2017; De Serio et al., 2018; Van Rooijen and Ghisalberti, 2018; Wang et al., 2018; Sonnenwald et al., 2019; Stewart et al. 2019; Zhang et al., 2019; Penna et al., 2022) evaluating and predicting different flow properties (roughness, resistance, turbulence structures, velocity distribution…etc.), few studies on the prediction of discharge capacity, based on traditional 1-D methods, have been observed in the literature (Kiczko et al., 2020).

Because the classical 1-D methods, such as the DCM method, are simple and easy to apply for modelling stage-discharge relations in compound channels, in this study, we try to adopt the Interacting Divided Channel Method (IDCM) proposed by Huthoff et al. (2008), for compound channels with floodplains without large-scale roughness elements (such as vegetation stems), to predict the discharge of a partly vegetated channel. The peculiarity of the IDCM method is that it includes the effects of lateral momentum transfer, which improves the reliability of discharge predictions. The novelty of this study is the consideration of both large-scale roughness elements (consisting of vegetation stems) and a curved-division interface plane by applying the IDCM method.

To make the model operational, a procedure to follow for the prediction of the zonal and total discharges of a partly vegetated channel is proposed (Sect. 2.2). This proposed model is very simple to apply because it depends on the characteristic variables of a partly vegetated channel that practitioners can easily define.

2. Theoretical considerations

The flow configuration considered in this study addresses uniform flow in a very large rectangular channel, of total width B, partially covered with an array of emergent, rigid, circular, and rough steel cylinders. This morphology is representative of emergent vegetation like reeds, bamboos, rushes, and many other trees of cylindrical rigid trunks (sometimes have well-arranged distribution in floodplains). Representing channel with vegetation patches, the array of cylinders is mounted on the central channel bottom over a full width of $2b_o$. Two unobstructed symmetrical side regions, each of width b, are present near the side walls of the channel. The cylinders were arranged in a square configuration and spaced with a distance s. The cylinders have the same diameter d and height h. Figure 1 shows a definition sketch of the considered problem. Since the flow field is symmetrical to the axis of the channel, we focus only on the flow in the half of the channel cross-section. Figure 1a shows that, along the y-transversal direction in half cross-section, the turbulent flow is characterized by two main regions: an obstructed region and an unobstructed region (White and Nepf, 2007; Ben Meftah et al., 2014; Ben Meftah and Mossa, 2016). The flow velocity in the obstructed/vegetated region, zone I in Figure 1, is indicated by U_1 (defined as the average pore velocity over time and space). The unobstructed region is divided into sub-zones: i) a free-stream zone, indicated by zone II near the side wall, where the flow reaches a full and constant velocity U_2, and ii) a zone of shear layer, indicated by zone III, in which U continuously increases from a velocity O(U_1) at the interface ($y = 0$) to the full velocity U_2. The flow velocities U and U_2 are the depth- and time-averaged velocity in each transversal position y.

The total flow resistance of the considered configuration is composed of three main components: i) the boundary shear stress (surface skin resistance), including bed and side wall stresses of the channel, ii) the additional drag caused by vegetation (drag form), and iii) the apparent shear stress, due to lateral momentum exchange at the interface between the obstructed and unobstructed areas. The apparent shear stress is usually significantly greater than the boundary

153 shear stress of the main channel (Helmiö, 2004, White and Nepf, 2007). Since the flow
154 hydrodynamic structures of the considered configuration (consisting of a main area, constituted by
155 the unobstructed region, of high velocities, and a subarea, obstructed by vegetation, of low
156 velocities) are very similar to those of a compound channel, the Interacting Divided Channel
157 Method (IDCM), proposed by Huthoff et al. (2008), is physically adaptable to partly vegetated flow
158 configuration. Tang (2019), applying the IDCM method with an inclined interface plane between
159 the mean channel and floodplains, also observed a significant improvement of the predicted
160 discharge compared to classical DCM method with vertical interface.
161
162 ***2.1. Adaptation of the Interacting Divided Channel Method (IDCM)***
163 Due to the great similarity between the flow hydrodynamic structures (presence of main
164 subsection of largest velocity, subsections of lowest velocity, development of a shear layer at the
165 interface between subsections) in compound and partly vegetated channels, in this study, we adapt
166 the IDCM method by Huthoff et al. (2008) based on the concept of apparent shear stress at an
167 arbitrary curved inclined interface plane between the obstructed and unobstructed regions. Figure 2
168 shows a descriptive scheme (cross-section of zone III) of the curved inclined interface plane. The
169 curved line originates from the bottom boundary layer at the intersection between zone I and zone
170 III ($y = y_m$) and ends at the free surface flow, at the intersection between zone III and zone II, where
171 y_m is the effective shear layer origin. The curved line separates the cross-section area A_3 of zone III
172 into subareas of cross-sections A_{a3} (subject of apparent shear stress) and A_{b3} (subject of boundary
173 shear stress). To simplify the calculation of the length of the curved line and the surfaces A_{a3} and
174 A_{b3}, the curved line has been replaced by two segments EO and OG, which intersect at point O
175 located on the diagonal (dashed line in Figure 2) of section A_3. Note that by changing the position of
176 point O along the diagonal of section A_3, it is possible to obtain the different classic-dividing-
177 interface-planes used in the DCM method: vertical (when EO equal to the flow depth H), diagonal

178 (when $EO = OG$), and horizontal (when EO equal to the width of the shear layerδ). The horizontal
179 interface plane is not applicable for this study because the obstructed and unobstructed regions have
180 the same flow depth. In Figure 2, k and k' indicate the vertical and transversal distances of point O
181 from the channel bottom and the zone II-III interface, respectively.

182 The momentum balance per unit length in the streamwise direction of channel subareas,
183 separated by the curved interface, as shown in Figure 1b, and defined in detail in Figure 2, can be
184 written as:

185

$$\rho g A_{23} S = \rho f_{23} {U_{23}}^2 P_{23} + \tau_a h' \quad (1)$$

$$\rho g A_{13} S = \rho f_{13} {U_{13}}^2 P_{13} + F_d - \tau_a h' \quad (2)$$

186

187 The left-hand sides of Eqs. (1) and (2) represent the streamwise component of the gravitational
188 force per unit length in the unobstructed and obstructed subareas of cross-sections A_{23} and A_{13}. The
189 first terms on the right-hand side of Eqs. (1) and (2) represent the boundary shear forces per unit
190 length along the wetted perimeters of the cross-sections A_{23} and A_{13}. The second term, F_d, on the
191 right-hand side of Eq. (2) represents the vegetated-induced drag force per unit length. The last terms
192 on the right-hand side of Eqs. (1) and (2) represent the apparent shear force per unit length along the
193 interface curved plane between the subareas of cross-sections A_{23} and A_{13} (Tang, 2019). In Eqs. (1)
194 and (2), ρ is the water density, g is the gravitational acceleration, $A_{23} = A_{b3} + A_2$ and $A_{13} = A_{a3} + A_1$
195 are the cross-sectional areas delimited by the interface curved plane, A_1 and A_2 are the cross-
196 sectional areas of zone I and zone II, respectively, S is the free surface slope, f_{23} and f_{13} are
197 respectively the frictional factors of the subareas A_{23} and A_{13}, U_{13} and U_{23} are the mean velocities in
198 the cross-sections A_{13} and A_{23}, respectively, P_{13} and P_{23} are the wetted perimeters (excluding the
199 interface length) relative to the cross-sections A_{13} and A_{23}, respectively, τ_a is the apparent shear
200 stress acting at the interface curved plane, and $h' \approx EO + OG$ (Figure 2) is the interface length.

The vegetated-induced drag force per unit length F_d can be expressed, using the drag coefficient for a single cylinder C_d, as:

$$F_d = \frac{1}{2}\rho C_d N b_o H d {U_1}^2 \tag{3}$$

where N is the vegetation density. According to previous studies (e.g., Huthoff et al.; 2008, Tang, 2019; Singh and Tang, 2020) the interfacial apparent shear stress is directly proportional to the difference in squared velocities U_{23} and U_{13} of the mean and obstructed subareas and can be expressed as:

$$\tau_a = \frac{1}{2}\rho\gamma\left({U_{23}}^2 - {U_{13}}^2\right) \tag{4}$$

where γ is an interface coefficient to be determined.

Substituting the expression of the apparent shear stress, Eq. (4), into Eq. (1) and after some arrangement and simplification we get an expression of the mean velocity U_{23} as:

$${U_{23}}^2 = {U_{23,0}}^2 - \frac{1}{2}\gamma\epsilon_{23}\left({U_{23}}^2 - {U_{13}}^2\right) \tag{5}$$

where

$${U_{23,0}}^2 = \frac{gR_{23}S}{f_{23}} \tag{6}$$

$$\epsilon_{23} = \frac{h'}{f_{23}P_{23}} \tag{7}$$

219 The substitution of Eq. (4) into Eq. (2) leads to the following expression of U_{13}:

220

$$U_{13}{}^2 = U_{13,0}{}^2 + \frac{1}{2}\gamma\epsilon_{13}\left(U_{23}{}^2 - U_{13}{}^2\right) \tag{8}$$

221

222 where

223

$$U_{13,0}{}^2 = \frac{gR_{13}S}{f_{13}} - \frac{F_d}{\rho f_{13}P_{13}} \tag{9}$$

$$\epsilon_{13} = \frac{h'}{f_{13}P_{13}} \tag{10}$$

224

225 To adapt the IDCM method by Huthoff et al. (2008) to partly vegetated channel, the novelty of this
226 study lies in the consideration of the vegetation-drag effect (not addressed in previous studies) in
227 the expression of $U_{13,0}$, as shown in Eq. (9).

228 By subtracting Eq. (8) from Eq. (5), we obtain the following expression of the squared
229 velocity difference:

230

$$U_{23}{}^2 - U_{13}{}^2 = \frac{U_{23,0}{}^2 - U_{13,0}{}^2}{\left[1 + \frac{1}{2}\gamma(\epsilon_{23} + \epsilon_{13})\right]} \tag{11}$$

231

232 After the substitution of Eq. (11) in Eqs. (5) and (8), one obtains the following unified
233 equations for U_{23} and U_{13}:

234

$$U_{23}{}^2 = U_{23,0}{}^2 - \frac{\frac{1}{2}\gamma\epsilon_{23}}{1 + \frac{1}{2}\gamma(\epsilon_{23} + \epsilon_{13})}\left(U_{23,0}{}^2 - U_{13,0}{}^2\right) \tag{12}$$

$$U_{13}{}^2 = U_{13,0}{}^2 + \frac{\frac{1}{2}\gamma\epsilon_{13}}{1+\frac{1}{2}\gamma(\epsilon_{23}+\epsilon_{13})}\left(U_{23,0}{}^2 - U_{13,0}{}^2\right) \quad (13)$$

235

236 In Eqs. (6) and (9), $R_{23} = A_{23}/P_{23}$ and $R_{13} = A_{13}/P_{13}$ are respectively the hydraulic radii of the
237 subarea of the main channel of cross-section A_{23} and the obstructed one of cross-section A_{13}. R_{23} and
238 R_{13} can be calculated as follows:

239

$$R_{23} = \frac{\left(1 - \frac{y_m}{b} - \lambda\frac{\delta}{b}\right)H}{1 - \frac{y_m}{b} + \beta' r_a} \quad (14)$$

$$R_{13} = \frac{\left[(1-\varphi)C_r + \frac{y_m}{b} + \lambda\frac{\delta}{b}\right]H}{(1-\varphi)C_r + \frac{y_m}{b} + \beta'' r_a} \quad (15)$$

240

241 where $\lambda = A_{a3}/A_3$ is a cross-sectional ratio of zone III, $\beta' = 0$ if the unobstructed area is not in
242 contact with channel side walls and $\beta' = 1$ if it is in contact with one of the channel side walls
243 (Figure 1), $r_a = H/b$ is the aspect ratio of the unobstructed area of width b (Figures 3 and 4), $\varphi =$
244 $N\pi d^2/4 = \pi ad/4$ is the solid fraction of cylinders, $a = Nd$ is the total frontal area per unit array, and
245 C_r is a contraction ratio, defined as the ratio of the obstructed-area width b_o to the width of the
246 unobstructed area b ($C_r = b_o/b$), $\beta'' = 0$ if the obstructed area is not in contact with channel side-
247 walls and $\beta'' = 1$ if it is in contact with one of the channel side-walls.

248 The interface length *h'*, which appears in Eqs. (7) and (10), can be calculated based on
249 Figure 2. The distance *OF* along the diagonal can be determined as: $OF = \alpha(H^2 + \delta^2)^{1/2} = (k^2 +$
250 $k'^2)^{1/2}$, where $0 \leq \alpha \leq 1$ is a factor of proportionality to the total diagonal length. Using Figure 2, we
251 can also find that $k' = (\delta/H)k$, $k = OF/[1 + (\delta/H)^2]^{1/2}$, $EO = [k^2 + (\delta - k')^2]^{1/2}$ and $OG = [k'^2 + (H -$
252 $k)^2]^{1/2}$. Finally, the expression of *h'* will be determined as:

253

$$h' = H \qquad \text{when } \alpha = 1 \tag{16}$$

$$h' = \sqrt{k^2 + (\delta - k')^2} + \sqrt{k'^2 + (H - k)^2} \qquad \text{when } 0 < \alpha < 1 \tag{17}$$

254

255 Referring to Figure 2, we can also find the expressions of A_{a3}, A_{b3} and the ratio λ,
256 considering that $A_3 = \delta H$, as:

257

$$A_{b3} = \frac{1}{2}(k\delta + k'H) \tag{18}$$

$$\lambda = \frac{A_{a3}}{A_3} = \frac{\delta H - \frac{1}{2}(k\delta + k'H)}{\delta H} = 1 - \alpha \tag{19}$$

258

259 ***2.2. Procedure of calculation***

260 The procedure to follow for the prediction of the zonal discharge and total discharge of a
261 partly vegetated channel is summarized as follows:
262 Step 1: the process begins with a detailed determination of the different characteristics of the partly
263 vegetated channel, as shown in Figure 1. The difficulty here is how to define the y_m and δ. This will
264 be discussed below in Sect. 4.1.
265 Step 2: calculate the interface length h', using Eq. (17) after calculating k and k' with a given value
266 of α. In this step, we can also calculate the value of λ, using Eq. (19).
267 Step 3: calculate the hydraulic radii R_{23} and R_{13}, using Eqs. (14) and (15), respectively.
268 Step 4: calculate the coefficients $\in_{23}$ and $\in_{13}$, using Eqs. (7) and (10), respectively. Herein, the
269 frictional factors will be calculated based on Manning's formulas as: $f_{23} = g(n_{23})^2(R_{23})^{-1/3}$ and $f_{13} =$
270 $g(n_{13})^2(R_{13})^{-1/3}$. The equivalent values of the manning coefficients n_{23} and n_{13} depend on the nature
271 of materials constituting the solid boundaries of each subarea.

Step 5: calculate the zonal mean velocities $U_{23,0}$ and $U_{13,0}$, using Eqs. (6) and (9), respectively. The wetted perimeters are determined as: $P_{23} = b - y_m + \beta' H$ and $P_{13} = (1 - \varphi)b_o + y_m + \beta'' H$. The vegetated-induced drag force F_d (Eq. 4) will be calculated by defining a drag coefficient C_d and by assuming a value of $U_1 = U_{13,0}$, and therefore Eq. (9) becomes as follows:

$$U_{13,0}{}^2 = \frac{gR_{13}S}{f_{13}\left(1 + \frac{\frac{1}{2}C_d a b_o H}{f_{13}P_{13}}\right)} \tag{20}$$

Note that the subscript 0 in $U_{13,0}$ indicates that the interface stress is not considered (interface coefficient $\gamma = 0$) and the solution is presented in terms of the flow velocity obtained with the classical DCM method. Therefore, $U_{13,0}$ is approximately of order U_1.

Step 6: calculate the predicted zonal mean velocities U_{23} and U_{13} based on Eqs. (12) and (13), respectively, with a given value of the coefficient γ.

Step 7: calculate the predicted zonal and total discharges as:

$$Q_1 = U_{13}A_1 = Q_o \tag{21}$$

$$Q_2 = U_{23}A_2 \tag{22}$$

$$Q_3 = U_{13}A_{a3} + U_{23}A_{3b} = [\lambda U_{13} + (1 - \lambda)U_{23}]A_3 = U_3 A_3 \tag{23}$$

$$Q_u = Q_2 + Q_3 = U_u(A_2 + A_3) \tag{24}$$

$$Q_T = (2 - \beta'')(Q_1 + Q_2 + Q_3) \tag{25}$$

where $Q_1 = Q_o$ is the discharge in zone I (obstructed by the vegetation), the cross-section area of zone I is determined as: $A_1 = [(1 - \varphi)b_o + y_m]H$, Q_2 is the discharge in zone II (free-stream), Q_3 is the discharge in zone III (shear layer), U_3 the mean velocity in zone III, Q_u is the discharge in the

unobstructed region (zone II-III), U_u the mean velocity in the unobstructed region, Q_T is the channel total discharge.

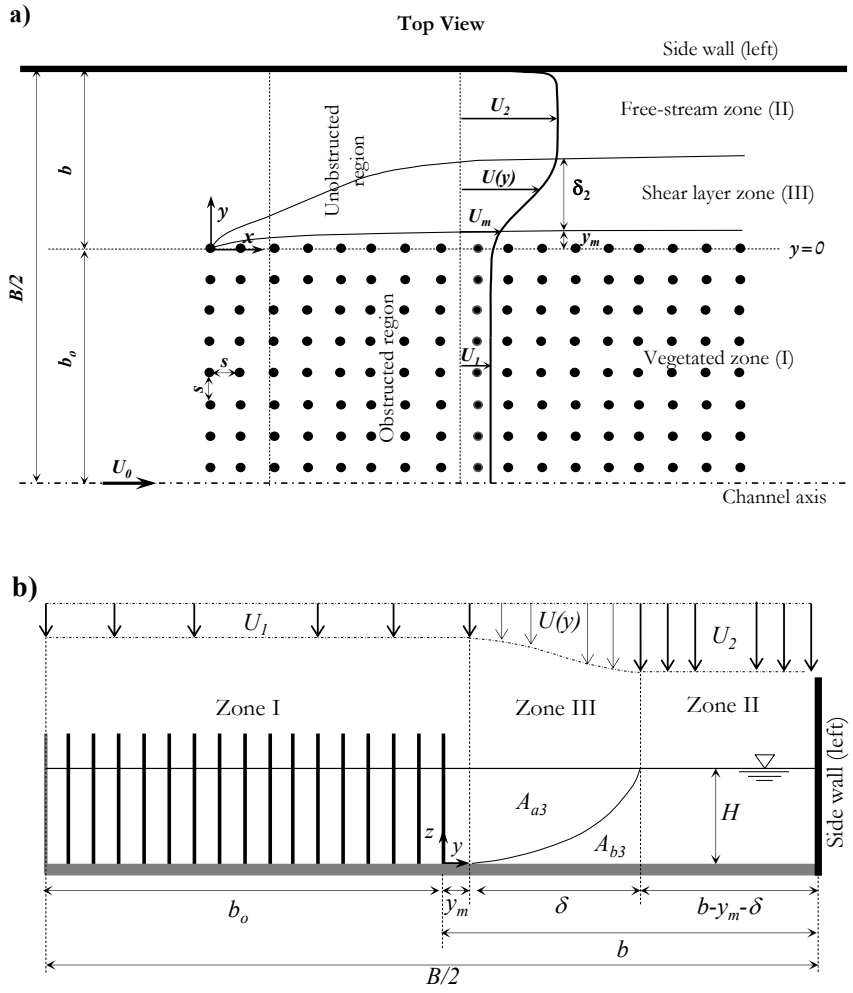

Figure 1. Problem description at the interface between the vegetated and non-vegetated domains: a) top view of the experimental area with different flow zones, b) front view of the three flow zones and their characteristic velocity profiles with subdivision of the cross-section of zone III into A_{b3} and A_{a3}. (x, y, z) are the longitudinal, transversal, and vertical coordinates, respectively.

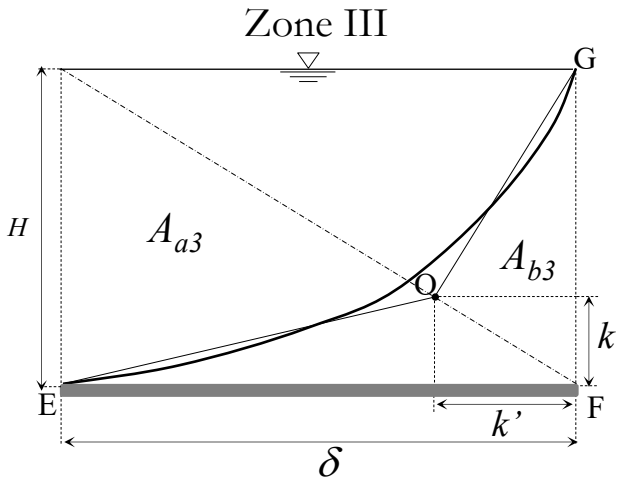

299

300 **Figure 2.** Descriptive scheme of the curved interface plane. The bold solid line represents the curved interface.

301

302 ## 3. Experimental method

303 The experiments on a partly vegetated rectangular channel were carried out at the Coastal
304 Engineering Laboratory (L.I.C.) of the Department of Civil, Environmental, Building Engineering
305 and Chemistry at the Polytechnic University of Bari, Italy. The channel consists of base and lateral
306 walls made of glass. The channel is 15 m long, 4 m large and 0.4 m deep. The water is supplied
307 from a large-downstream steel tank to an upstream one, using a Flygt centrifugal electric pump, in a
308 closed hydraulic circuit. A side-channel spillway of adjustable height is installed in the upstream
309 tank to maintain constant flow-head condition. The overflow water is drained through a pipeline to
310 the downstream tank. The pumped and overflow water discharges are measured using two
311 electromagnetic flowmeters mounted on the channel's hydraulic circuit. The difference between the
312 two flow discharges defines the total discharge of the channel. To create a smooth flow transition
313 from the upstream tank to the flume, a set of stilling grids are installed in the upstream tank to
314 dampen inlet turbulence. The channel is equipped with an upstream and a downstream gate to
315 define both the depth and the mean velocity of the flow (Figure 3).

316 The vegetation array consists of vertical, rigid, circular, and threaded steel cylinders. The
317 cylinder height, h, is 0.31 m and its diameter, d, is 0.003 m. The cylinders were inserted into a

318 bottom plywood plaque 9.0 m long, 4.0 m wide and 0.02 m thick. The array of cylinders is partially
319 mounted in the central part of the channel, forming the experimental area of 3 m long and $2b_o$
320 width. Two symmetric lateral regions immediately adjacent to the channel sides, each of width b,
321 are left for free flow circulation (see Figure 1). Four experimental configurations, based on the
322 contraction ratio C_r, were investigated, varying b and b_o. The 3 m extension of the plywood plaque,
323 both upstream and downstream of the array of cylinders, and its taping to the channel bottom helps
324 to minimize flow disturbance. Cylinders are regularly arranged and spaced longitudinally and
325 transversally with the same distance $s = 5.0$ cm, giving rise to a density, N, of 400 cylinders/m^2.

326 The origin of the x-axis ($x = 0$) is taken at the upstream edge of the array of cylinders, while
327 that of the y-axis ($y = 0$) is taken at the array edge (interface between the obstructed and
328 unobstructed domains). The z-axis has its origin at the channel bottom. Since the flow within the
329 canopy is turbulent and highly heterogeneous at the scale of the individual cylinder, the
330 measurement of the three-dimensional flow is of crucial importance. The three flow velocity
331 components were accurately measured using an Acoustic Doppler Velocimeter (ADV)-Vectrino,
332 manufactured by Nortek. Using the ADV-Vectrino, a velocity range of ±0.30 m/s, a vertical
333 extension of sampling volume of 7 mm, a sampling rate of 150 Hz and a time of acquisition of 2
334 min were established. The acquired data were filtered based on Tukey's method and the bad
335 samples (SNR < 15 and correlation coefficient < 70%) were removed.

336 Detailed information on the measurements performed is summarized in Table 1, where Re_d
337 $= U_1 d/\nu$ is the Reynolds number based on cylinder diameter, $Re_2 = U_2 H/\nu$ is the Reynolds number
338 based on flow depth, Q_m is the measured main channel discharge, ν is the water kinematic viscosity,
339 and δ^* is a modified width of zone III (explained below in Sect. 4.1). In addition to the experimental
340 data of the present study, some data obtained in previous studies are also considered and illustrated
341 in Table 1. The White and Nepf's (2007, 2008) data were obtained in a laboratory flume 13 m long
342 and 1.2 m wide, partially obstructed with a 40 cm wide emergent array (adjacent to a side wall of

the flume) of 6.5 mm diameter wooden circular cylinders (Figure 4). The cylinder density, the flow depth and the flow discharge were varied during the experimentation. The measurements of flow velocity were made with a Laser Doppler Velocimetry (LDV) system. The data of Caroppi (2018) were obtained in a rectangular channel 8 m long, 0.40 m wide and 0.4 m deep. A lateral area of width 0.1625 m along the entire length of the flume was obstructed by an array of aligned emergent cylinders of 4.5 mm diameter (Figure 4). Different cylinder packing densities, flow depth and flow rates were tested. Instantaneous velocity measurements were performed with a SonTek Micro Acoustic Doppler Velocimeter (ADV).

Table 1: Initial experimental conditions and some parameters of the investigated runs: [1, 2] calculated using Eqs. (26) and (27), respectively. NI stands not identified. ♦Discharges estimated using velocity distribution.

Runs	φ (-)	$C_d a$ (cm^{-1})	C_r (-)	H (cm)	r_a (-)	U_1 (cm/s)	U_2 (cm/s)	Re_d (-)	Re_2 (-)	δ (cm)	y_m (cm)	$^1\delta^\blacklozenge$ (cm)	^2C_d (-)	Q_m (l/s)
Present study														
R0	0.0028	0.015	3.21	28.0	0.59	7.47	18.17	182	$4.1x10^4$	28.02	1.87	32.29	2.36	100.0
R1	0.0028	0.015	3.21	25.0	0.53	7.98	21.79	240	$5.4x10^4$	22.59	2.90	31.70	2.03	100.0
R2	0.0028	0.017	3.21	22.0	0.46	9.04	24.81	197	$4.0x10^4$	25.50	2.40	31.03	2.32	100.0
R3	0.0028	0.014	3.21	18.0	0.38	10.91	30.94	278	$4.7x10^4$	25.49	2.47	29.98	2.07	100.0
R4	0.0028	0.012	3.21	14.0	0.29	13.90	38.53	365	$4.7x10^4$	24.81	1.89	28.67	1.99	100.0
R5	0.0028	0.014	3.21	12.0	0.25	18.80	43.05	465	$4.3x10^4$	24.43	2.48	27.87	2.05	100.0
R6	0.0028	0.016	1.05	28.0	0.29	5.67	15.29	138	$3.5x10^4$	44.65	3.14	46.60	2.07	100.0
R7	0.0028	0.016	1.05	25.0	0.26	6.80	16.79	165	$3.4x10^4$	39.49	4.11	45.38	2.06	100.0
R8	0.0028	0.015	1.05	22.0	0.23	8.11	18.94	197	$3.4x10^4$	35.35	4.50	44.01	2.03	100.0
R9	0.0028	0.015	1.05	18.0	0.18	8.91	23.46	218	$3.4x10^4$	36.70	4.60	41.86	1.95	100.0
R10	0.0028	0.014	1.05	14.0	0.14	8.20	30.98	203	$3.6x10^4$	34.95	3.79	39.17	1.85	100.0
R11	0.0028	0.015	0.36	14.0	0.09	7.40	26.65	185	$3.1x10^4$	32.10	7.01	34.96	1.72	100.0
R12	0.0028	0.014	0.36	12.0	0.08	7.48	31.95	193	$3.3x10^4$	32.91	6.83	32.46	1.64	100.0
R13	0.0028	0.015	0.36	18.0	0.12	9.41	19.79	239	$3.0x10^4$	43.63	6.02	39.04	1.80	100.0

R14	0.0028	0.016	0.36	22.0	0.15	7.17	15.52	184	$2.9x10^4$	35.98	5.82	42.30	1.87	100.0
R15	0.0028	0.016	0.36	25.0	0.17	7.32	13.47	189	$2.9x10^4$	44.09	4.85	44.37	1.90	100.0
R16	0.0028	0.015	0.16	25.0	0.14	7.80	11.85	191	$2.4x10^4$	36.76	2.35	33.68	1.91	100.0
R17	0.0028	0.014	0.16	18.0	0.10	8.30	18.32	207	$2.7x10^4$	34.49	3.14	27.45	1.73	100.0
R18	0.0028	0.014	0.16	12.0	0.07	8.21	29.22	209	$3.0x10^4$	26.94	3.99	19.75	1.59	100.0
R19	0.0028	0.016	0.16	28.0	0.16	7.50	11.06	194	$2.7x10^4$	40.98	2.45	35.83	1.85	100.0
White and Nepf (2007, 2008)														
I	0.020	0.092	0.50	6.8	0.09	2.21	17.68	131	$1.1x10^4$	15.95	4.12	20.83	2.71	10.6♦
II	0.020	0.092	0.50	10.4	0.13	1.74	21.69	103	$2.1x10^4$	19.07	5.12	24.57	2.09	NI
III	0.020	0.092	0.50	13.8	0.17	1.89	23.97	112	$3.0x10^4$	19.86	4.64	27.06	1.80	NI
IV	0.045	0.285	0.50	6.6	0.08	1.25	17.34	74	$1.0x10^4$	16.69	1.54	20.34	2.76	9.8♦
V	0.045	0.242	0.50	5.3	0.07	0.25	3.82	15	$1.8x10^3$	16.90	1.71	18.41	6.12	NI
VI	0.045	0.255	0.50	6.0	0.08	0.84	12.32	50	$6.7x10^3$	18.20	1.15	19.50	3.36	6.4♦
VII	0.100	2.430	0.50	6.6	0.08	0.43	16.82	25	$1.0x10^4$	16.50	2.21	19.82	2.79	9.2♦
VIII	0.100	2.740	0.50	5.5	0.07	0.15	5.85	9	$2.9x10^3$	15.53	2.09	18.21	4.92	NI
IX	0.100	2.040	0.50	6.8	0.09	0.25	9.05	15	$5.6x10^3$	15.20	2.01	20.08	3.69	NI
X	0.100	1.770	0.50	7.8	0.10	0.89	29.59	53	$2.1x10^4$	17.84	2.24	21.29	2.01	18.8♦
XI	0.100	2.430	0.50	13.9	0.17	0.41	22.02	24	$2.8x10^4$	21.54	2.84	26.37	1.86	10.6♦
Caroppi (2018)														
R-I	0.025	0.219	0.68	8.4	0.35	9.50	84.20	431	$7.1x10^4$	10.20	2.10	10.71	1.56	15.2
R-II	0.025	0.192	0.68	10.2	0.43	10.10	91.20	94	$1.9x10^4$	9.90	2.14	11.22	2.99	19.5
R-III	0.025	0.139	0.68	13.5	0.57	11.90	100.70	529	$1.3x10^5$	11.10	2.42	11.95	1.27	29.4
R-IV	0.013	0.097	0.68	8.5	0.36	14.20	87.00	638	$7.4x10^4$	9.50	2.13	10.78	1.53	17.3
R-V	0.013	0.084	0.68	10.6	0.45	15.30	90.40	677	$9.4x10^4$	10.40	2.26	11.36	1.43	21.7
R-VI	0.013	0.069	0.68	13.6	0.57	16.90	99.60	755	$1.3x10^5$	11.20	2.44	12.01	1.27	31.8
R-VII	0.013	0.051	0.68	8.8	0.37	19.50	81.90	864	$7.1x10^4$	9.40	1.93	10.87	1.57	17.3
R-VIII	0.013	0.045	0.68	10.6	0.45	21.00	84.90	970	$9.2x10^4$	8.80	1.88	11.36	1.44	21.7
R-IX	0.013	0.035	0.68	13.5	0.57	23.80	97.50	1098	$1.3x10^5$	10.40	2.20	11.99	1.27	31.7
R-X	0.006	0.020	0.68	13.3	0.56	31.10	93.40	1420	$1.3x10^5$	10.60	2.31	11.96	1.31	31.7
R-XI	0.003	0.012	0.68	12.2	0.51	39.70	92.10	1831	$1.2x10^5$	10.40	2.20	11.75	1.34	31.7

R-XII	0.002	0.007	0.68	11.1	0.47	51.70	94.00	2473	$1.1x10^5$	8.20	1.57	11.50	1.34	31.7
R-XIII	0.001	0.005	0.68	8.8	0.37	65.51	98.80	2761	$8.1x10^4$	8.20	1.22	10.90	1.48	31.7

354

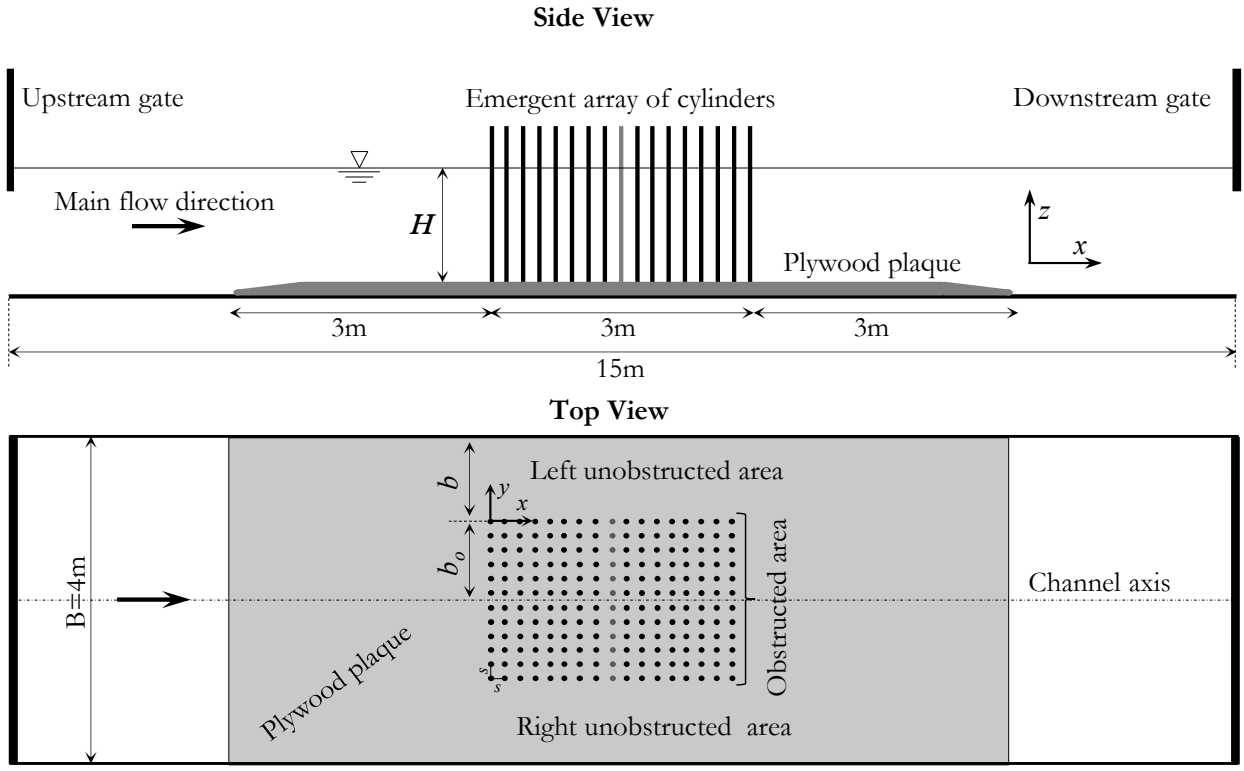

355

356 **Figure 3**. General sketch of the laboratory flume with the experimental area. The vegetation array is not adjacent to any

357 side wall of the channel: $\beta' = 1$ and $\beta'' = 0$.

358

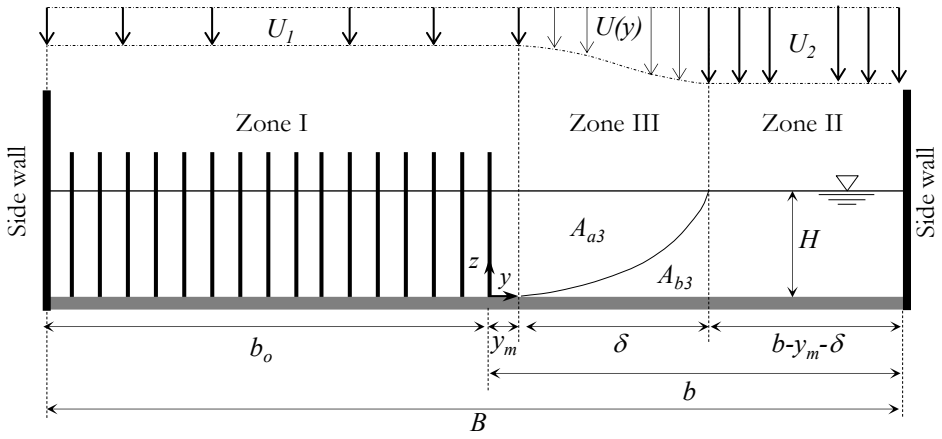

359

360 **Figure 4**. Front view of the channel cross-section in White and Nepf (2007, 2008) and Caroppi (2018), the vegetation

361 array is adjacent to a side wall of the channel: $\beta' = 1$ and $\beta'' = 1$.

362

4. Results and discussion

4.1. Prediction of shear layer width and vegetation drag coefficient

The shear boundary layer, zone III in Figures 1 and 4, is characterized by a width δ, which originates at a lateral distance y_m from the vegetation edge. These two characteristic parameters (δ, y_m) explicitly depend on the flow-vegetation interaction dynamics (White and Nepf, 2007, 2008; Ben Meftah and Mossa, 2016, Li et al., 2022), and their determination requires detailed information on the lateral distribution of the flow velocity. According to previous studies (e.g., White and Nepf, 2007, 2008; Ben Meftah and Mossa, 2016), y_m is usually significantly small compared to δ. To make the procedure of discharge predicting easily applicable, we have combined y_m and δ into a new δ^*(= y_m + δ) length scale. With this consideration, the width of zone III becomes δ^* instead of δ, including the length scale y_m. Figure 5 shows the trend of δ^*/b as a function of the dimensionless parameter (1-φ)$C_r r_a$. The data plotted in Figure 5 refer to the present study and previous studies by White and Nepf (2007, 2008) and Caroppi (2018), as shown in Table 1. Figure 5 indicates a clear increasing trend of δ^*/b with the increase of (1-φ)$C_r r_a$. A logarithmic regression analysis of these data leads to an expression for predicting δ^* as follows:

$$\frac{\delta^*}{b} = 0.11Ln[(1-\varphi)C_r r_a] + 0.61 \quad (26)$$

The drag coefficient C_d represents a key parameter to calculate the total drag force by vegetation. Determining C_d is a challenging task due to its complex dependence on the macro and microstructure of vegetation arrays as well as flow characteristics (Ben Meftah, 2013; Huai et al., 2019; Liu et al., 2020). In the last decades, several experimental, theorical and numerical studies were conducted to predict the drag coefficient in vegetated channel flows. Recently, Liu et al. (2020) provided a good summary of several methodologies used to measure the drag coefficient, C_d,

386 of emergent vegetation in open channel flows, presenting a comprehensive list of existing predictors
387 of C_d. The authors also proposed an innovative robust predictor of C_d using genetic programming
388 (GP) and machine learning (ML) techniques based on natural selection of large series of published
389 data.

390 To find an easy expression predicting the drag coefficient, in this study, we aim to find out a
391 relationship between C_d and the Reynolds number $Re_{23,0} = U_{23,0}R_{23}/\nu$ of the main channel area,
392 where $U_{23,0}$ and R_{23} calculated based on Eqs. (6) and (14), using δ^* instead of δ and annulling y_m (y_m
393 = 0). It is worth mentioning that $Re_{23,0}$ is expressed as a function of variables that practitioners can
394 easily define. In Figure 6, we plot the experimentally estimated values of C_d (Table 1), obtained in
395 the present study and previous studies by White and Nepf (2007, 2008) and Caroppi (2018), versus
396 $Re_{23,0}$. C_d shows a decreasing trend with an increase of $Re_{23,0}$. The best fit to the data leads to the
397 following expression to predict the drag coefficient:

$$C_d = 182\left(Re_{23,0}\right)^{-0.47} \tag{27}$$

398

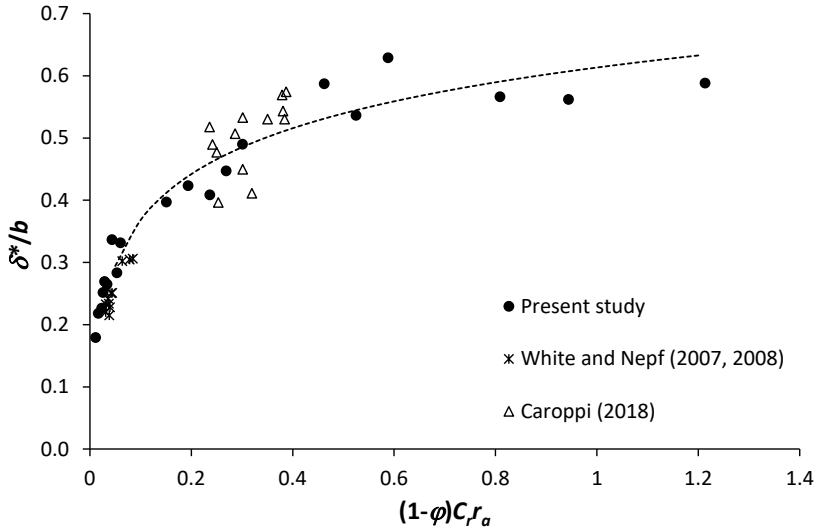

399

400 **Figure 5**. Trend of normalized length scale δ^*/b as a function of $(1-\varphi)C_r r_a$.

401

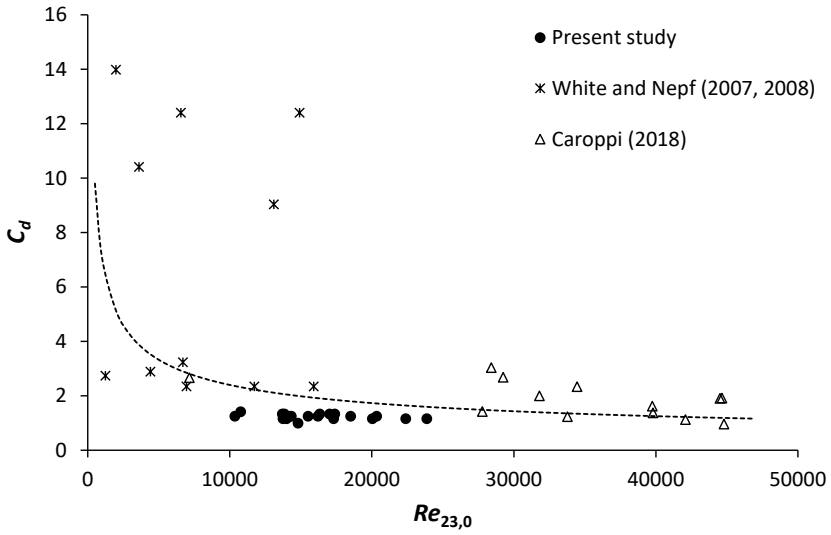

Figure 6. Trend of drag coefficient C_d as a function of $Re_{23,0}$.

4.2. Results of discharge prediction by applying IDCM with a curved interface

All the experiments of this study and the previous studies, used to predict the flow discharges, were of steady, uniform and fully developed flow. The channels have rectangular cross-sections made of glass/Plexiglas and are characterized by fixed beds. The roughness was identified in terms of a Manning coefficient n, considered constant and determined based on the nature of the material constituting each laboratory channel. Since the channel bed of the present study is covered with a plywood plaque (Figure 3), an equivalent Manning roughness coefficient of n = 0.013 was assumed, whereas a value of n = 0.01 was considered for both previous studies by White and Nepf (2007, 2008) and Caroppi (2018). The free surface slope S, which is theoretically equal to the bed slope with a uniform flow, was determined based on the measured flow velocity U_2 (of constant value) through zone II. The average value (of all runs) of S is almost equal to $2\text{x}10^{-4}$, $1\text{x}10^{-4}$ and $2\text{x}10^{-3}$ for the present study, the studies by White and Nepf (2007, 2008) and that by Caroppi (2018), respectively.

Figure 7 shows a comparison between the measured and predicted (applying the IDCM method) total discharges for the present study (Figure 7a) and the previous studies by White and Nepf (2007, 2008) and Caroppi (2018), as shown in Figures 7b and 7c, respectively. It is worth

421 mentioning that the results depicted in Figure 7 were obtained after testing different values of the
422 curved interface line *h'* to reach the best performance, by varying the values of α (between 0 and 1)
423 and γ. Furthermore, in the calculation procedure (Sect. 2.2) δ^* was used instead of δ, annulling y_m,
424 and C_d was estimated using Eq. (27). For the present study, the values of $\alpha = 0.20$ ($\lambda = 0.80$) and γ
425 $= 0.023$ lead to the most accurate discharge prediction. A good performance of the IDCM method
426 was also obtained with a similar value of γ (= 0.020) in a previous study by Huthoff et al. (2008),
427 predicting flow discharges in a compound channel. For the previous studies by White and Nepf
428 (2007, 2008) and Caroppi (2018), the best IDCM-performances were achieved with values of ($\alpha =$
429 0.39, $\gamma = 0.037$) and ($\alpha = 0.10$; $\gamma = 0.012$), respectively.
430 According to Tang (2019), the mean absolute percentage error (MAPE) of predicted
431 discharge has already been used as a criterion for the method's accuracy and calculated as follows:
432

$$E_Q = \frac{|Q_p - Q_m|}{Q_m} \times 100 \tag{28}$$

433
434 where E_Q is the percentage error of the predicted discharge, Q_p is the predicted discharge and Q_m is
435 the measured discharge. In Figure 7, the E_Q-values of the different runs are shown above the
436 histograms. For the present study (Figure 7a), E_Q shows for most runs a value less than 8%, except
437 for 5 runs where it varies between 13% and 23%. The average value of E_Q for the 20 runs, shown in
438 Figure 7a, is slightly below 6%, indicating the good performance of the IDCM method. White and
439 Nepf (2007, 2008) in their original papers only indicated the range of discharge variation of their
440 experiments. The five measured discharges, presented in Figure 7b, were estimated based on
441 available detailed data (Runs I, IV, VI, VII, X) of transversal distribution of the streamwise velocity
442 depicted in the study by White and Nepf (2008). Despite the uncertainty in estimating the White
443 and Nepf's (2007, 2008) measured discharges, E_Q indicates four values less or equal to 9% and an
444 average value of order 10%. The predicted discharges, shown in Figure 7c, also indicate good

445 accuracy. Most of the values of E_Q vary between 0% and 10%, giving an average value of 7% for
446 all runs.

447 The application of the IDCM method with $\alpha = 0.20$ and $\gamma = 0.023$ (values that led to the
448 best IDCM-performance with the data of this study) to the White and Nepf's (2007, 2008) and
449 Caroppi's (2018) data yields an average value of E_Q almost equals to 11% and 10%, respectively.
450 Here we notice that there is a slight variation of the average value of E_Q from 10% and 7%, as best
451 IDCM-performance with the data of White and Nepf (2007, 2008) and Caroppi (2018), to 11% and
452 10% (obtained with $\alpha = 0.20$ and $\gamma = 0.023$), respectively. This allows us to consider a value of $\alpha =$
453 0.23 ($\lambda = 0.77$) and $\gamma = 0.024$ (obtained averaging the α- and γ-values of best performances for the
454 three analyzed datasets) for the combined data. Hereafter we indicate by "combined data" the set of
455 data of the present study and the studies of White and Nepf (2007, 2008) and Caroppi (2018) treated
456 together. With $\alpha = 0.23$ and $\gamma = 0.024$, we obtained an average value of E_Q of almost 6% with the
457 present study, 11% for both studies of Nepf (2007, 2008) and Caroppi (2018) and 9% for the
458 combined data.

459 Figure 8 shows the results of the predicted and measured total discharges for the different
460 datasets (present study's, White and Nepf's (2007, 2008) and Caroppi's (2018) data), applying the
461 DCM method with the same values of α as in Figure 7. Note that with the DCM method, the
462 contribution of the apparent shear stress is not considered, i.e., $\gamma = 0$, as indicated by the subscript 0
463 in $Q_{T,0}$. Figure 8 shows a significant underestimation of the predicted discharges compared to those
464 measured. Most values of E_Q are higher than 30% for the three datasets used for analysis. E_Q is of
465 average value approximately equal to 29%, 30% and 33% for the present study with $\alpha = 0.20$, the
466 studies by White and Nepf (2007, 2008) with $\alpha = 0.39$ and that by Caroppi (2018) with $\alpha = 0.10$,
467 respectively. With $\alpha = 0.23$, E_Q is almost equal to 28%, 35% and 25% for the present study, the
468 studies by White and Nepf (2007, 2008) and the study by Caroppi (2018), respectively, and it is
469 approximately 29% for the combined data. However, it was observed that E_Q significantly

decreases with a high value of α. E_Q reaches a minimum average value approximately equal to 7%, 14% and 3% for the present study with $\alpha = 0.90$ ($\lambda = 0.10$), the studies by White and Nepf (2007, 2008) with $\alpha = 0.92$ ($\lambda = 0.08$) and that of Caroppi (2018) with $\alpha = 0.62$ ($\lambda = 0.38$), respectively. With $\alpha = 0.81$ (average of the three α-values of 0.90, 0.92 and 0.62), for the combined data, E_Q is of average value approximately equal to 13%. It is worth remembering that, with $\alpha = 0.23$ and $\gamma = 0.024$, the average value of E_Q applying the IDCM method for the combined data is almost 9%. This implies that the IDCM method predicts more accurately the flow discharges than the DCM method. Table 2 shows a comparison between the performance of the IDCM and DCM methods.

Figure 9 shows a comparison between the predicted and measured normalized discharges in the three different subareas, i.e., zone I, zone II, zone III. Both predicted and measured discharges are normalized by the total predicted discharge Q_T. The data presented in Figure 9 were obtained applying the IDCM method with a curved interface plane of $\alpha = 0.23$ ($\lambda = 0.77$) and $\gamma = 0.024$. The zonal predicted discharges were calculated using Eqs. (21-23). Figure 9a shows the normalized discharges in the obstructed region, zone I. For all runs of the present study and the studies by White and Nepf (2007, 2008) and Caroppi (2018), the IDCM method shows an overestimation of the discharge Q_1. The data scattering in Figure 9a may be due to the high uncertainty of both the measured velocity U_1 and the drag coefficient estimation. Figure 9b shows the data of Q_2/Q_T, discharge in the free stream-zone (zone II), subject of constant velocity U_2. In this zone, the IDCM method underestimates the discharge Q_2 by a value around 20%, as shown by the deviated dashed line from the perfect fitted line (solid line). The good collapse of data onto a single curve in Figure 9b reflects more precision in measuring the flow velocity U_2. Figure 9c presents the normalized discharge, Q_3/Q_T, in the shear layer zone (zone III). Despite the slight data scattering shown in Figure 9c, the predicted and measured discharges indicate a good correlation, where most data collapse at and close to the perfect fitted line (solid line).

494 It should be underlined that with $\alpha = 0.50$ we obtain the classic diagonal divisional channel method.
495 This division method showed low performance in predicting the total discharges compared to the
496 curved division. With $\alpha = 0.50$, for the combined data, the IDCM method with $\gamma = 0.02$ gives an
497 average value of E_Q approximately equal to 16%, while the DCM method showed a value of almost
498 18%.
499
500 **Table 2:** Performance of IDCM compared to DCM methods with curved interface plane. The left column of DCM
501 represents the results obtained with the values of (α , λ) which give better performance with IDCM method. The right
502 column of DCM illustrates the results of better performance of DCM with curved interface.

Runs			**IDCM**		**DCM *(γ = 0)***	**DCM *(γ = 0)***		
	α (-)	λ (-)	γ (-)	E_Q (%)	E_Q (%)	α (-)	λ (-)	E_Q (%)
Present study	0.20	0.80	0.023	5.87	28.71	0.90	0.10	6.40
White and Nepf (2007, 2008)	0.20	0.80	0.023	11.48	36.31	0.90	0.10	14.00
Caroppi (2018)	0.20	0.80	0.023	10.04	27.25	0.90	0.10	20.63
Present study	0.39	0.61	0.037	12.60	21.44	0.92	0.08	6.66
White and Nepf (2007, 2008)	0.39	0.61	0.037	9.78	30.41	0.92	0.08	13.65
Caroppi (2018)	0.39	0.61	0.037	18.05	15.73	0.92	0.08	22.08
Present study	0.10	0.90	0.012	9.86	32.58	0.62	0.38	13.29
White and Nepf (2007, 2008)	0.10	0.90	0.012	13.27	39.32	0.62	0.38	22.95
Caroppi (2018)	0.10	0.90	0.012	6.73	32.93	0.62	0.38	3.41
Combined data	0.23	0.77	0.024	9.48	29.47	0.81	0.19	12.74

503
504
505
506
507
508

509

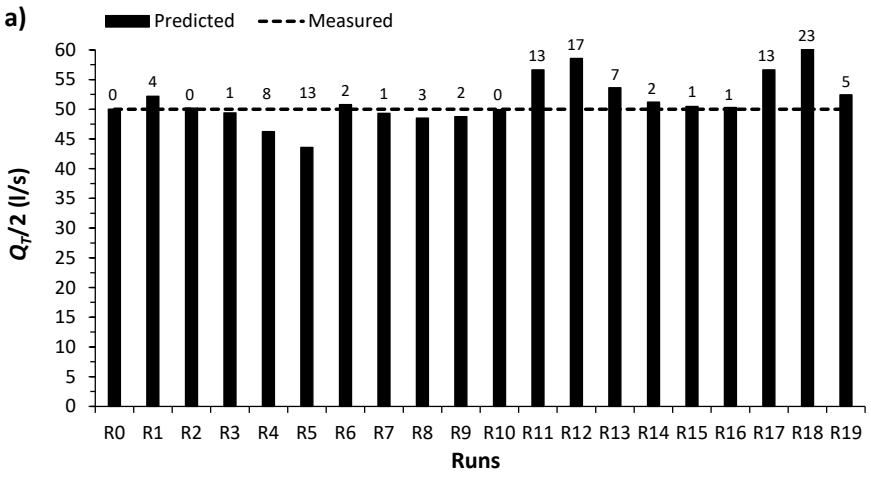

510

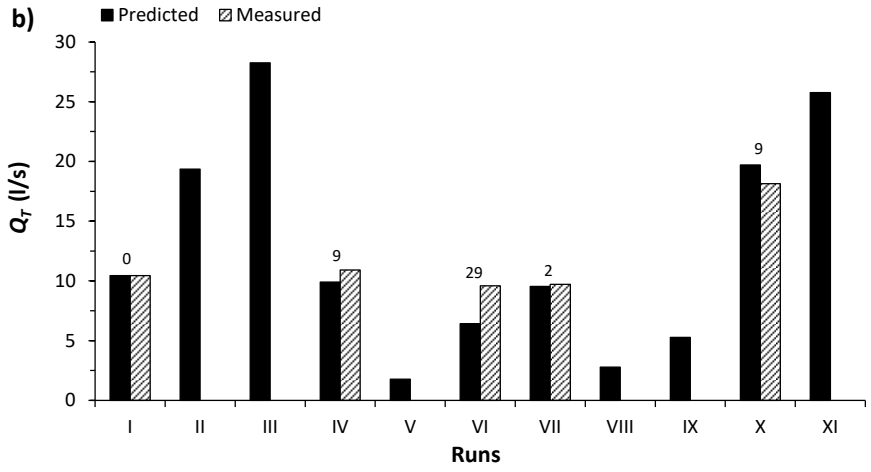

511

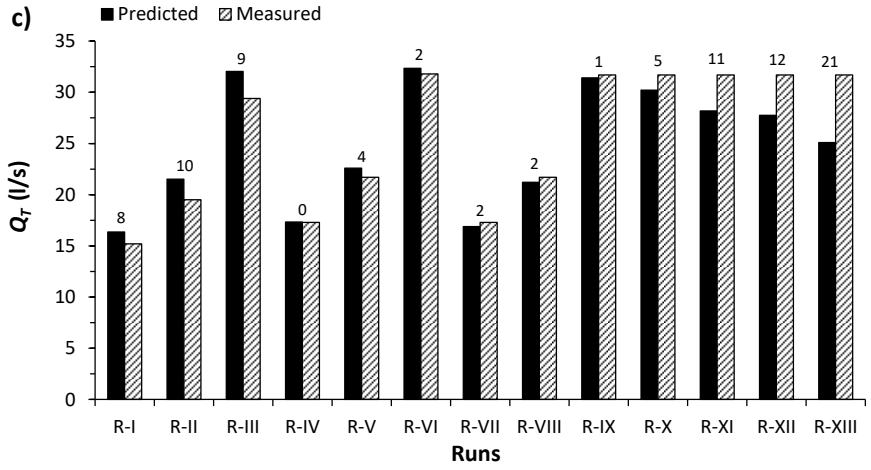

512

513 **Figure 7**. Predicted compared to measured total discharges using the IDCM method with a curved interface plane: a)
514 present study with $\alpha = 0.20$ ($\lambda = 0.80$) and $\gamma = 0.023$, b) studies by White and Nepf (2007, 2008) with $\alpha = 0.39$ ($\lambda =$
515 0.61) and $\gamma = 0.037$, c) study by Caroppi (2018) with $\alpha = 0.10$ ($\lambda = 0.90$) and $\gamma = 0.012$. The values above the
516 histograms are of E_Q, for each run.

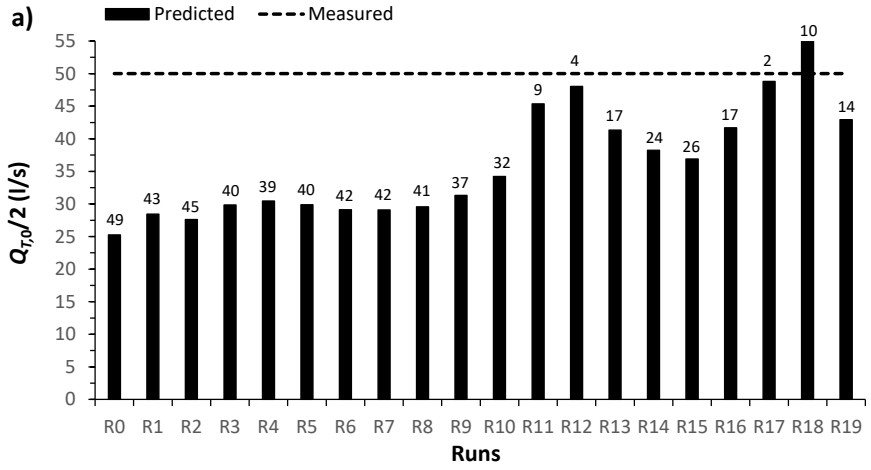

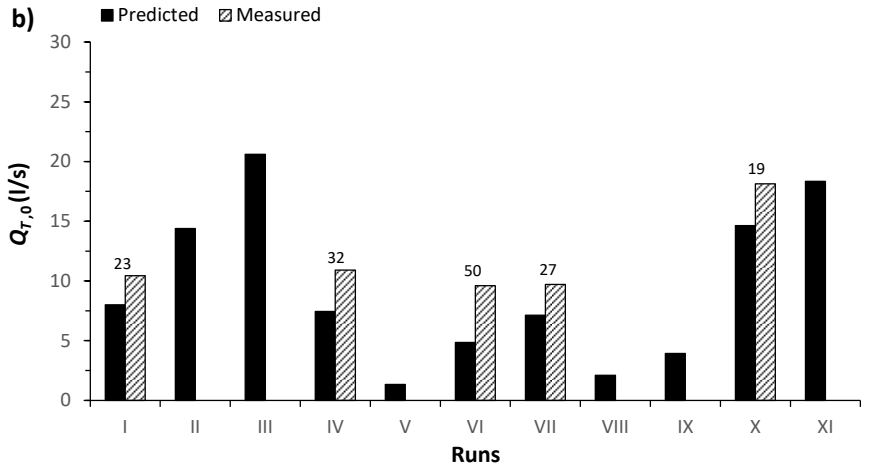

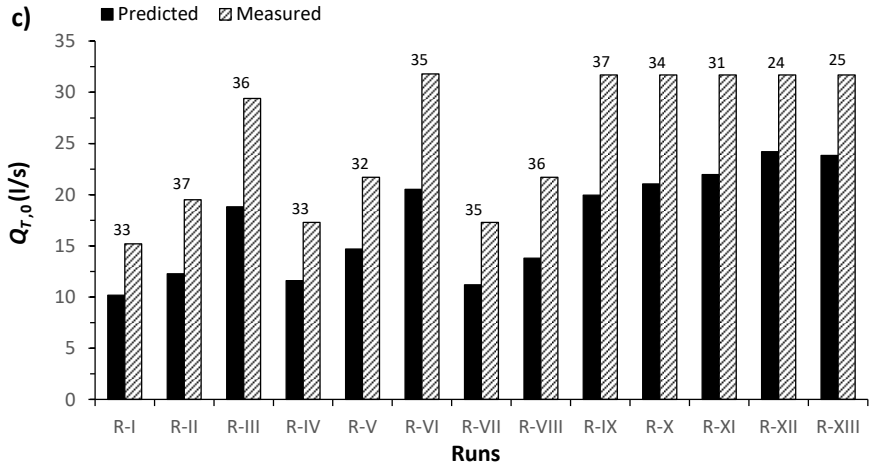

Figure 8. Predicted compared to measured total discharges using the DCM method ($\gamma = 0$), with a curved interface plane: a) present study with $\alpha = 0.20$ ($\lambda = 0.80$), b) studies by White and Nepf (2007, 2008) with $\alpha = 0.39$ ($\lambda = 0.61$), c) study by Caroppi (2018) with $\alpha = 0.10$ ($\lambda = 0.90$).

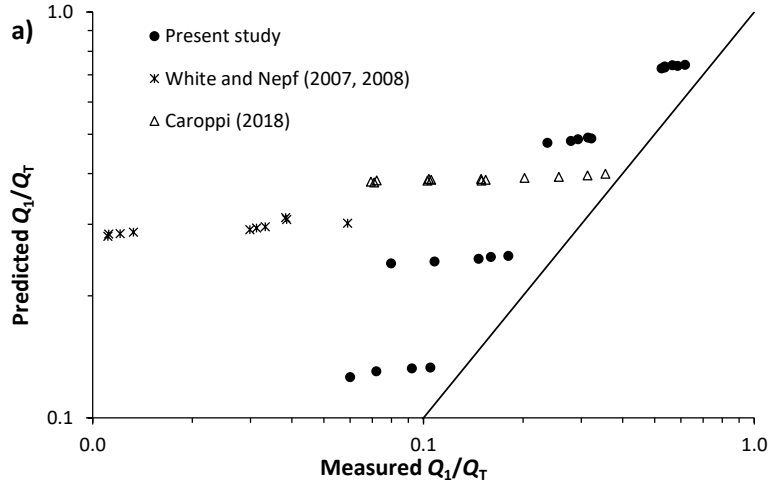

524

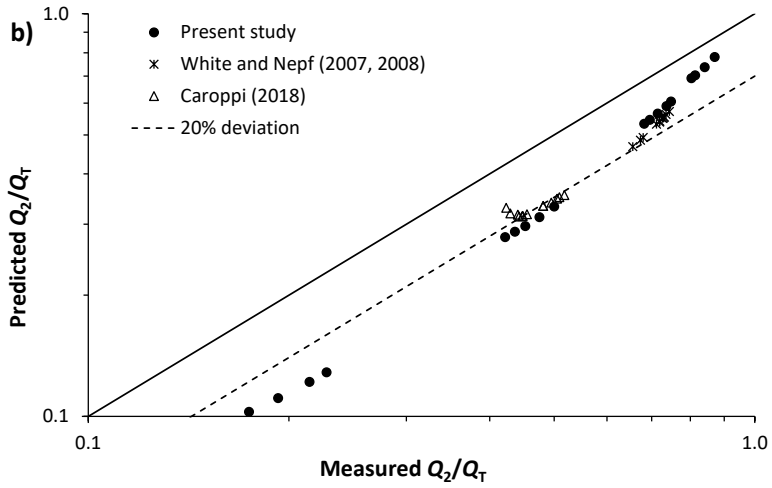

525

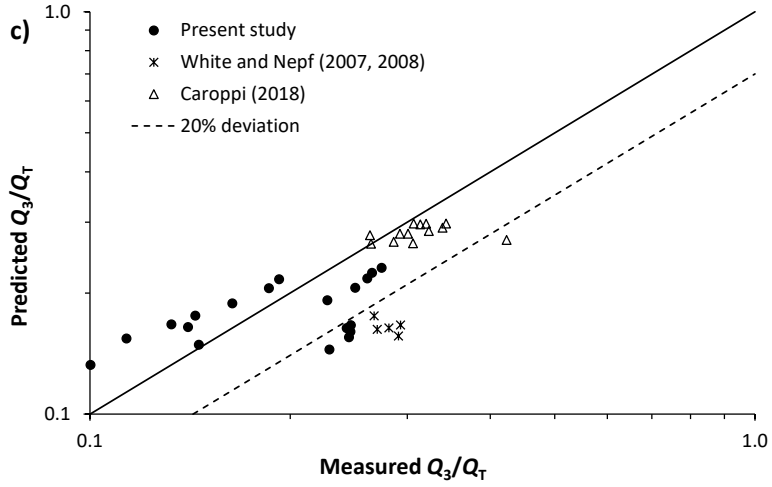

526

527 **Figure 9**. Zonal predicted compared to measured normalized discharges obtained by the IDCM method with a curved
528 interface plane of overall values of $\alpha = 0.23$ ($\lambda = 0.77$) and $\gamma = 0.024$: a) Q_1/Q_T in zone I, b) Q_2/Q_T in zone II, and c)
529 Q_3/Q_T in zone III, Q_T is the total predicted discharge. The solid line denotes the perfect fitted line, while the dashed line
530 indicates a 20% deviation from the perfect fitted line.

531

4.3. Dependence of zonal discharges to the cross-section characteristic parameters

With the aim of finding practical expressions to predict the zonal flow discharges, we conducted further analysis based on the channel-sectional characteristic parameters (Figures 1 and 4). In Figure 10a, we plot the normalized predicted discharge Q_1/Q_T of the obstructed region (zone I) versus the dimensionless parameter $(1-\varphi)C_r r_a^{0.1}$. It is worth point out that the predicted discharges presented in Figure 10 are results of the IDCM method with a curved interface of α = 0.23 and γ = 0.024. Figure 10a shows a perfect collapse of the data, from the different studies, onto a single increasing curve. A logarithmic regression of the combined data yields an empirical expression, of coefficient of determination R^2 = 0.99, to predict the discharge in the obstructed region Q_1 as follows:

$$\frac{Q_1}{Q_T} = 0.20Ln[(1-\varphi)C_r r_a{}^{0.10}] + 0.50 \quad (29)$$

Figure 10b shows the normalized predicted discharge Q_2/Q_T in the free-stream region (zone II) plotted against the parameter $(1-\varphi)C_r r_a^{0.5}$. Figure 10b points out that Q_2/Q_T systematically decreases as $(1-\varphi)C_r r_a^{0.5}$ increases, following an almost perfect trend. A logarithmic regression of the combined data also leads to an empirical expression, of coefficient of determination R^2 = 0.99, for the discharge Q_2 in the free-stream region as follows:

$$\frac{Q_2}{Q_T} = -0.17Ln[(1-\varphi)C_r r_a{}^{0.50}] + 0.20 \quad (30)$$

552 Since by continuity $Q_T = Q_1 + Q_2 + Q_3$, an expression to predict the discharge Q_3 in the
553 interface between the obstructed and unobstructed regions (zone III) can be easily obtained, based
554 on Eqs. (29) and (30) as:
555

$$\frac{Q_3}{Q_T} = -0.03Ln[(1-\varphi)C_r {r_a}^{-2.17}] + 0.30 \quad (31)$$

556
557 The prediction of zonal discharges is of crucial importance for many reasons, i.e.,
558 determination of the flow velocity in each compartment, expectation of possible erosion or
559 deposition of solid materials, river restoration and management, hydraulic capacity improvement,
560 flow impact on ecological health. The discharge predictors, shown in Eqs (29-31), are expressed as
561 a function of variables that practitioners can easily define, making them very simple to apply for
562 partly vegetated channels, especially after having defined the total discharge Q_T.
563
564
565
566
567
568

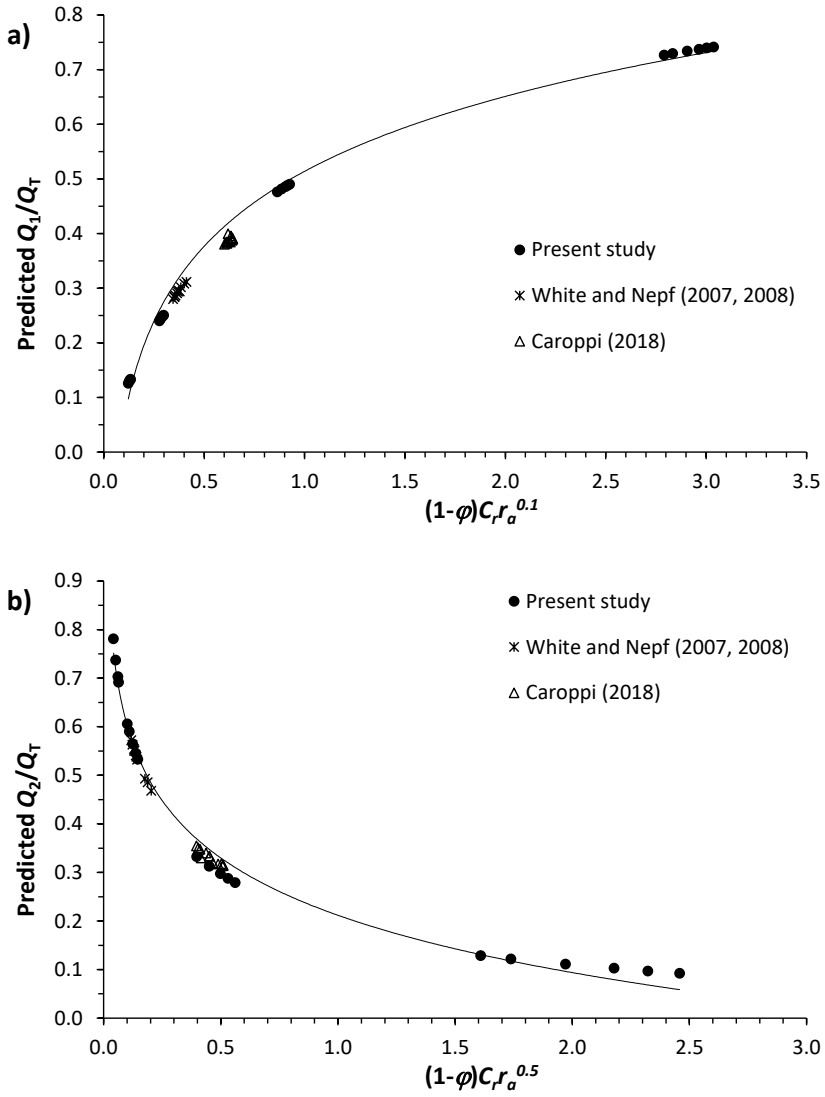

569

570

571 **Figure 10**. Dependence of zonal predicted discharges to characteristic parameters of channel cross-section: a)

572 dependence of Q_1/Q_T, in the obstructed zone I, to $(1-\varphi)C_r r_a^{0.1}$, b) dependence of Q_2/Q_T, in the free-stream zone II, to

573 $(1-\varphi)C r_a^{0.5}$. Q_T is the total predicted discharge. The solid line denotes the fitted trend of the combined data. IDSM

574 results with $\alpha = 0.23$ ($\lambda = 0.77$) and $\gamma = 0.024$.

575

576 ***4.4. Results of discharge prediction with vertical interface***

577 Based on the curved interface approach proposed in this study, the vertical interface occurs

578 when $\alpha = 1.00$ ($\lambda = 0.00$). Here, the peculiarity is that the length of the interface *h'* becomes equal

579 to the distance *EO* (see Figure 2), which is necessarily equal to the flow depth *H*. It has been

580 observed that by setting the value of $\alpha = 1$, the consideration of the apparent shear stress effect, i.e.,

581 $\gamma \neq 0$, has no impact on achieving better IDCM performance. The best performance in predicting the
582 flow discharges was obtained with a value of $\gamma = 0$, i.e., with the DCM method. Figure 11 illustrates
583 a comparison between the predicted and measured total discharges for the present study and
584 previous studies by White and Nepf (2007, 2008) and Caroppi (2018). For the present study (Figure
585 11a), most of the predicted discharges are comparable to those measured, with an E_Q ranging
586 between 1 and 12%. The average value of E_Q of all the 19 runs is approximately equal to 10%,
587 which is almost double that obtained applying the IDCM method with a curved surface of $\alpha = 0.20$
588 and $\gamma = 0.023$ (See Table 2). Figure 11b and 11c show significantly lower performances, compared
589 to the present study, analyzing White and Nepf's (2007, 2008) and Caroppi's (2018) data. E_Q
590 indicates an average value of approximately 12 and 28% with the dataset of White and Nepf (2007,
591 2008) and Caroppi (2018), respectively. The average value of E_Q for the combined data is of order
592 17%, against a value of 9% and 13% (Table 2) obtained applying the IDCM ($\alpha = 0.23$ and $\gamma =$
593 0.024) and DCM ($\alpha = 0.81$) with curved interface plane, respectively. This implies that the curved
594 divisional channel method shows better performance than classic vertical division.
595 Figure 12 shows the predicted versus measured total discharges obtained applying the
596 IDCM and DCM methods with curved and vertical interface planes. Both the IDCM and DCM with
597 a curved interface show better performance in predicting channel discharges than the DCM with a
598 vertical interface, which overestimates most discharges by more than 20%, as indicated by the
599 dashed line in Figure 12. With the consideration of a curved interface plane, the best performance
600 was achieved with the IDCM method, as can also be distinguished from Table 2.
601
602 ***4.5. Vortical structure in the shear layer region***
603 Analysis of the flow behavior in the shear layer region (zone III), as shown in Figure 13,
604 shows the development of a clockwise vortex of a length scale of order δ (width of zone III). Figure
605 13 indicates that the secondary current cell occupies the largest cross-section area of zone III, which

606 is subject to considerable transverse momentum transfer. This momentum transfer generates
607 considerable apparent resistance, affecting the flow velocity distribution and therefore the flow
608 discharge through this zone. The apparent resistance should be physically proportional to the cross-
609 section area subject to considerable transverse momentum transfer due to the dominated vortex
610 structure in zone III, giving rise to consider a curved interface (Figure 2) to better represent the
611 proportionality of this area (defined above as λ) to the total cross-section area of zone III, A_3. The
612 introduction of a curved interface approach is strongly confirmed by the best performance of the
613 IDCM method in predicting the flow discharges.
614
615
616
617
618
619
620
621
622
623
624
625

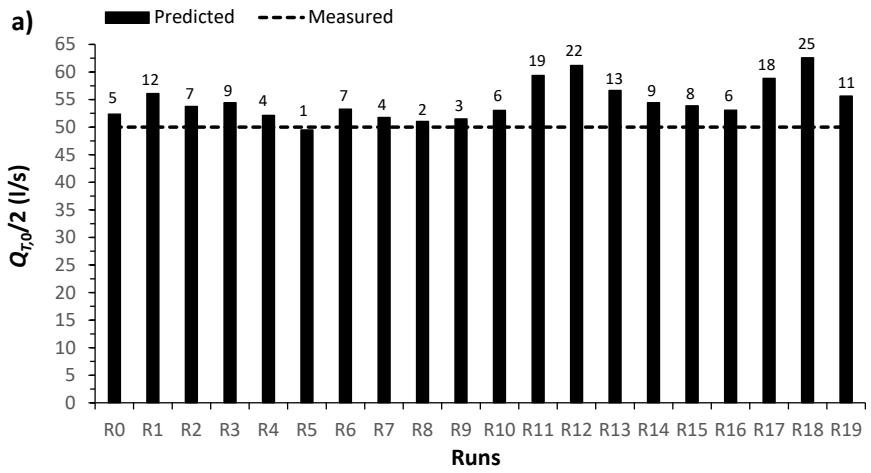

626

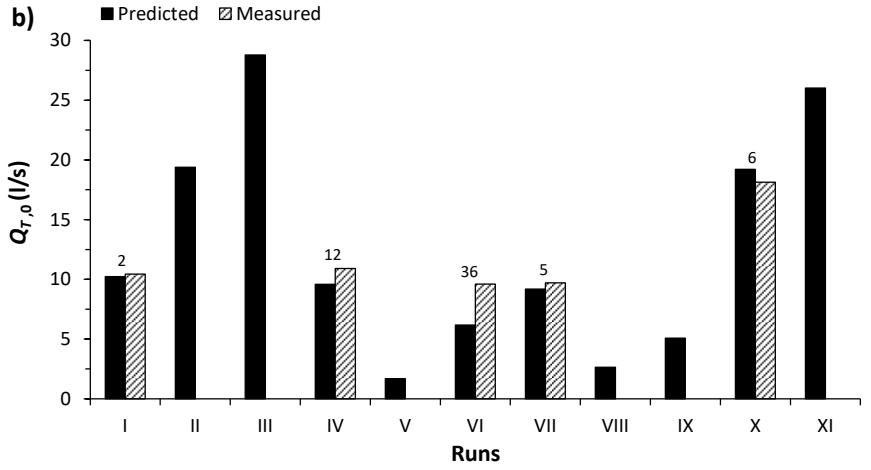

627

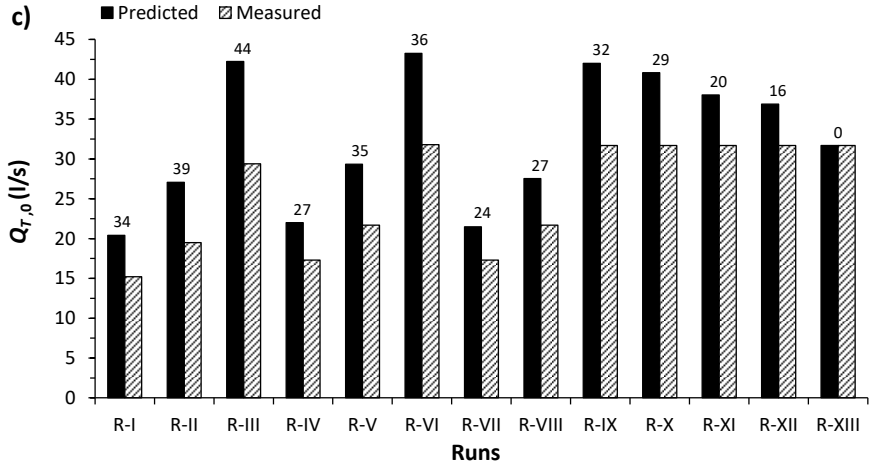

628

629 **Figure 11**. Predicted compared to measured total discharges using the DCM method ($\gamma = 0$) with vertical interface
630 plane of $\alpha = 1.00$ ($\lambda = 0.00$): a) present study, b) studies by White and Nepf (2007, 2008), and c) study by Caroppi
631 (2018).

632

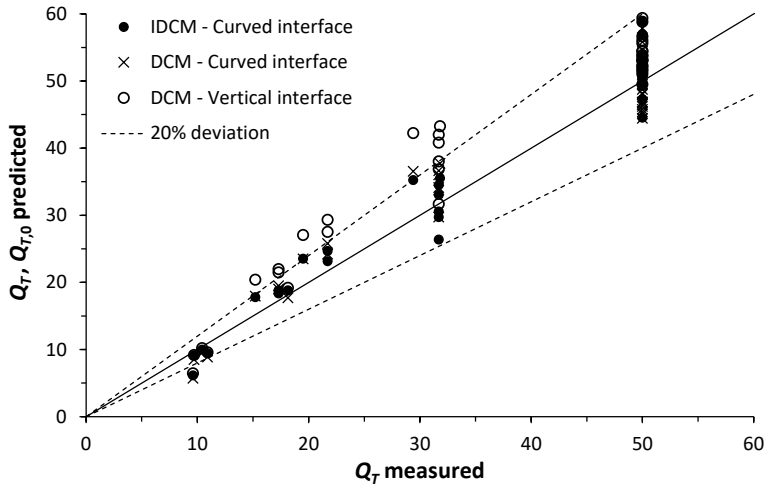

633

634 **Figure 12**. Predicted compared to measured total discharges for combined data. Data refer to best performance obtained
635 with curved interface applying the IDCM ($\alpha = 0.23$ and $\gamma = 0.024$) and DCM ($\alpha = 0.81$) and with vertical interface
636 applying the DCM ($\alpha = 1$). The solid line denotes the perfect trend between predicted and measured discharges. The
637 dashed lines indicate the deviation by ±20% from the perfect trend.

638

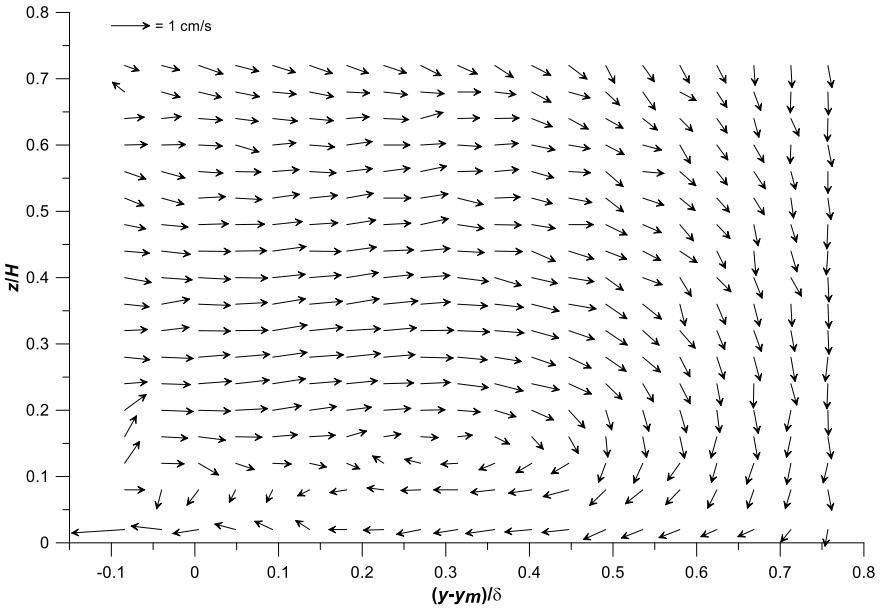

639

640 **Figure 13**. Secondary current cell through the shear layer region (zone III). A clockwise vortex of a length scale of
641 order the width δ of zone III is clearly observed. Data refers to run R1 of the present study.

642

643

644

645

5. Conclusions

In this study, we adopted for the first time the IDCM method to predict flow discharge in a partly vegetated channel with emergent rigid vegetation. Transverse momentum transfer was considered in terms of apparent shear stress, acting on a curved interface plane. In this study, the choice of a curved interface approach was justified by the dominance of a vortical structure in the shear layer region. It was observed that most of the interface area (zone III in this study) is subject to the development of a typical vortex of a length scale on the order of the width of this interface area. This study confirms that a curved divisional channel method better physically represents the effect of apparent resistance in the shear layer region.

The IDCM method applied with a curved interface leads to find practical analytical expressions of the flow velocity on the main and obstructed subsections of a partly vegetated channel, giving rise to discharge prediction. To make these expressions simple and easily applicable by practitioners, we proposed empirical formulas to predict the width of the interface zone and the drag coefficient due to vegetation stems (characteristic parameters essential for the calculation procedure). The IDCM applied with a curved interface plane is characterized by two free coefficients α (coefficient to define the interface curved length) and γ (interface coefficient for the apparent shear stress).

The flow discharge prediction based on laboratory experiments shows a sensitivity of the IDCM method to α and γ values. Comparison of the different analyzed datasets shows that the best IDCM-performance was achieved with values of α and γ in the range 0.10 - 0.39 and 0.012 - 0.037, respectively. The results of the combined data of the different laboratory experiments lead to better performance of IDCM with $\alpha = 0.23$ and $\gamma = 0.024$. The best performance of the DCM method was obtained with values of α ranging between 0.62 and 0.92 treating separately the data of the different studies and with $\alpha = 0.81$ for combined data. Based on the results achieved in this study, the IDCM method with a curved interface plane showed better performance in predicting the flow discharge in

671 partly vegetated channels than the DCM method. Furthermore, the IDCM method applied with a
672 curved interface also showed better performance than DCM with classic vertical or transversal
673 division methods.
674 In this study, we also proposed a series of expressions, easily applicable, to predict the zonal
675 discharges of the different characteristic subareas in a partly vegetated channel.
676 Further sophisticated experiments in partly vegetated channels are recommended for future
677 studies to determine more accurate values of the characteristic coefficients α and γ.
678

679 ## Acknowledgement

680 This study was carried out at the Coastal Engineering Laboratory (L.I.C) of the Polytechnic
681 University of Bari, Italy, Department of Civil, Environmental, Building Engineering and Chemistry.
682

683 ## Notations

A	Cross-sectional area (m^2)
a	Total frontal area (area exposed to the flow) per unit array (m^{-1})
B	Channel width (m)
b	Width of the unobstructed area (m)
b_o	Width of the obstructed area (m)
C_d	Drag coefficient (-)
C_r	Contraction ratio (-)
d	Cylinder diameter (m)
F_d	Drag force per unit length (N/m)
f	Darcy-Weisbach friction factor (-)
g	Gravity acceleration ($m.s^{-2}$)
H	Flow depth (m)
h	Cylinder height (m)
k, k'	Useful lengths for estimating the curved interface length (m)
N	Density of cylinders ($cylinders.m^{-2}$)
n	Manning coefficient ($m^{-1/3}.s$)
P	Wetted perimeter (m)
Q	Flow discharge ($m^3.s^{-1}$)
R	Hydraulic radius (m)
r_a	Aspect ratio (-)
Re	Reynolds number (-)
S	Free surface slope (-)

s	Space between cylinders (m)
U	Streamwise time-averaged velocity (ms^{-1})
U_1	Flow pore velocity inside the obstructed region (ms^{-1})
U_2	Free-stream velocity in the unobstructed area (ms^{-1})
x, y, z	Longitudinal, transversal and vertical coordinates, respectively (m)
y_m	Effective shear layer origin (m)
α, γ	Coefficient of proportionality (-)
β, β', β''	Constants to define the channel configurations (-)
δ, δ^*	Shear layer width (m)
λ	Cross-sectional ratio (-)
ρ	Water density ($kg.m^{-3}$)
τ_a	Apparent shear stress ($N.m^{-2}$)
φ	Volume solid fraction of the cylinders (-)
ν	Water kinematic viscosity ($m^2.s^{-1}$)

684

685 **References**

686 Ackers P., 1993. Flow formulae for straight two-stage channels. Journal of Hydraulic Research Vol.
687 31(4), 509-531. DOI: 10.1080/00221689309498874

688 Al-Khatib I., Dweik A.A. and Gogus M., 2012. Evaluation of separate channel methods for
689 discharge computation in asymmetric compound channels. Flow Measurement and Instrumentation
690 Vol. 24(4), 19-25. DOI: 10.1016/j.flowmeasinst.2012.02.004

691 Ben Meftah M. and Mossa M., 2013. Prediction of channel flow characteristics through square
692 arrays of emergent cylinders. Physics of Fluids Vol. 25, 045102. DOI: 10.1063/1.4802047

693 Ben Meftah, M., De Serio, F. and Mossa, M., 2014. Hydrodynamic behavior in the outer shear layer
694 of partly obstructed open channels, Phys. Fluids Vol. 26(6), 065102, 1-19. DOI: 10.1063/1.4881425

695 Ben Meftah, M., De Serio, F., Malcangio, D., Mossa, M. and Petrillo, A.F., 2015. Experimental
696 study of a vertical jet in a vegetated crossflow. J. Environ. Manage. Vol. 164, 19-31. DOI:
697 10.1016/j.jenvman.2015.08.035

698 Ben Meftah M. and Mossa M., 2016. Partially obstructed channel: Contraction ratio effect on the
699 flow hydrodynamic structure and prediction of the transversal mean velocity profile. Journal of
700 Hydrology Vol.542(11), 87-100. Doi: 10.1016/j.jhydrol.2016.08.057

701 Caroppi G., 2018. Turbulence in partly vegetated channels: Experiments with complex morphology
702 vegetation and rigid cylinders. Thesis submitted for the degree of PhD in Civil Systems
703 Engineering, fedOA Università degli Studi di Napoli Federico II, Napoli, December 2018.

704 Chen G., Huai W., Han J. and Zhao M., 2010. Flow structure in partially vegetated rectangular
705 channels. J. Hydrodyn. 22(4), 590–597. DOI: 10.1016/S1001-6058(09)60092-5

706 Cheng N.S. and Nguyen H.T., 2011. Hydraulic radius for evaluating resistance induced by
707 simulated emergent vegetation in open channel flows. Journal of Hydraulic Engineering Vol.
708 137(9), 995-1004. DOI: 10.1061/(asce)hy.1943-7900.0000377

709 De Serio F., Ben Meftah M., Mossa M. and Termini D., 2018. Experimental investigation on
710 dispersion mechanisms in rigid and flexible vegetated beds. Advances in Water Resources Vol.
711 120(10), 98-113. DOI: 10.1016/j.advwatres.2017.08.005

712 Farhadi H., Zahiri A., Reza Hashemi M. and Esmaili k., 2019. Incorporating a machine learning
713 technique to improve open-channel flow computations. Neural Computing and Applications Vol.
714 31, 909-921. DOI: 10.1007/s00521-017-3120-7

715 Farooq R., Ahmad W., Hashmi H.N. and Saeed Z., 2016. Computation of momentum transfer
716 coefficient and conveyance capacity in asymmetric compound channel. Arabian Journal for Science
717 and Engineering Vol. 41, 4225-4234. DOI: 10.1007/s13369-016-2173-8

718 Ghisalberti M. and Nepf H.M., 2004. The limited growth of vegetated shear layers. Water
719 Resources Research, Vol. 40, W07502, 1-12. DOI: 10.1029/2003WR002776

720 Ghisalberti M., 2010. The three-dimensionality of obstructed shear flows. Environmental Fluid
721 Mechanics Vol. 10(3), 329-343. DOI: 10.1007/s10652-009-9161-4

722 Hamidifar H., Keshavarzi A. and Omid M.H., 2016. Evaluation of 1-D and 2-D models for
723 discharge prediction in straight compound channels with smooth and rough floodplain Vol. 49, 63-
724 69. DOI: 10.1016/j.flowmeasinst.2016.05.007

725 Helmiö T., 2004. Flow resistance due to lateral momentum transfer in partially vegetated rivers.
726 Water Resources Research Vol. 40(5), W05206 (1-10). DOI: 10.1029/2004WR003058

727 Huai W.X., Zhang J., Katul G.K., Cheng Y.G., Tang X. and Wang W.J., 2019. The structure of
728 turbulent flow through submerged flexible vegetation. Journal of Hydrodynamics Vol. 31(2), 274-
729 292. DOI: 10.1007/s42241-019-0023-3

730 Huthoff W., Roos P.C., Augustijn C.M.A. and Hulscher S.J.M.H., 2008. Interacting divided
731 channel method for compound channel flow. Journal of Hydraulic Engineering Vol. 134(8), 1158-
732 1165. DOI: 10.1061/(ASCE)0733-9429(2008)134:8(1158)

733 Kiczko A., Västilä K., Koziol A., Kubrak J., Kubrak E. and Krukowski M., 2020. Predicting
734 discharge capacity of vegetated compound channels: uncertainty and identifiability of one-
735 dimensional process-based models. Hydrology and Earth System Sciences Vol. 24 (8), 4135-4167.
736 DOI: 10.5194/hess-24-4135-2020

737 Knight D.W. and Demetriou J.D., 1983. Flood plain and main channel flow interaction. Journal of
738 Hydraulic Engineering Vol. 109(8), 1073-1092. DOI: 10.1061/(ASCE)0733-
739 9429(1983)109:8(1073)

740 Lima A.C. and Izumi N., 2014. On the nonlinear development of shear layers in partially vegetated
741 channels. Phys. Fluids Vol. 26 (8), 1-22. http://dx.doi.org/10.1063/1.4893676, 084109

742 Liu X. and Zeng Y., 2017. Drag coefficient for rigid vegetation in subcritical open-channel flow.
743 Environmental Fluid Mechanics Vol. 17(5), 1035-1050. DOI: 10.1007/s10652-017-9534-z

744 Li D., Liu M. and Huai W., 2022. Modeling transverse momentum exchange in partially vegetated
745 flow. Physics of Fluids Vol. 34, 025124. DOI: 10.1063/5.0081202

746 Liu M.Y., Huai W.X., Yang Z.H. and Zeng Y.H., 2020. A genetic programming-based model for
747 drag coefficient of emergent vegetation in open channel flows. Advances in Water Resources Vol.
748 140(1), 103582. DOI: 10.1016/j.advwatres.2020.103582

749 Mossa M., Ben Meftah M., De Serio F. and Nepf H.M., 2017. How vegetation in flows modifies the
750 turbulent mixing and spreading of jets. Scientific Reports Vol. 7, 6587. DOI: 10.1038/s41598-017-
751 05881-1

752 Myers W., 1978. Momentum transfer in a compound channel. Journal of Hydraulic Research Vol.
753 16(2), 139-150. DOI: 10.1080/00221687809499626

754 Myers W.R.C. and Brennan E.K., 1990. Flow resistance in compound channel, Journal of Hydraulic
755 Research Vol. 28 (2),141-155. DOI: 10.1080/00221689009499083

756 Naot D., Nezu I. and Nakagawa H., 1996. Hydrodynamic behavior of partly vegetated open
757 channels. Journal of Hydraulic Engineering Vol. 122(11), 625-633. DOI: 10.1061/(ASCE)0733-
758 9429(1996)122:11(625)

759 Nepf H.M., 1999. Drag, turbulence, and diffusion in flow through emergent vegetation. Water
760 Resources Research Vol. 35 (2), 479-489. DOI: 10.1029/1998WR900069

761 Parsaie A., Najafian S. and Yonesi H., 2016. Flow discharge estimation in compound open channel
762 using theoretical approaches. Sustainable Water Resources Management Vol. 2, 359-367. DOI:
763 10.1007/s40899-016-0063-6

764 Penna N., Coscarella F., D'Ippolito A. and Gaudio R., 2022. Effects of fluvial instability on the bed
765 morphology in vegetated channels. Environmental Fluid Mechanics Vol. 22, 619-644. DOI:
766 10.1007/s10652-022-09832-x

767 Pradhan S. and Khatua, K.K., 2020. Momentum transfer coefficients at the adjoining interfaces of a
768 compound channel. Flow Measurement and Instrumentation Vol. 75(10), 101792(1-12). DOI:
769 10.1016/j.flowmeasinst.2020.101792

770 Prinos P. and Townsend R.D., 1984. Comparison of methods for predicting discharge in compound
771 open channels. Advances in Water Resources Vol. 7(4), 180-187. DOI: 10.1016/0309-
772 1708(84)90016-2

773 Sonnenwald F., Stovin V. and Guymer I., 2019. Estimating drag coefficient for arrays of rigid
774 cylinders representing emergent vegetation. Journal of Hydraulic Research Vol. 57(4), 591-597.
775 DOI: 10.1080/00221686.2018.1494050

776 Stewart M.T., Cameron S.M., Nikora V.I., Zampiron A. and Marusic I., 2019. Hydraulic resistance
777 in open-channel flows over self-affine rough beds. Journal of Hydraulic Research Vol. 57(2), 183-
778 196. DOI: 10.1080/00221686.2018.1473296

779 Sellin R.H.J., 1964. A laboratory investigation into the interaction between the flow in the Channel
780 of a river and that over its flood plain. La Houille Blanche Vol. 50(7), 793-802. DOI:
781 10.1051/lhb/1964044

782 Singh P. and Tang X., 2020. Zonal and overall discharge prediction using momentum exchange in
783 smooth and rough asymmetric compound channel flows. Journal of Irrigation and Drainage
784 Engineering Vol. 146(9), 05020003(1-13). DOI: 10.1061/(ASCE)IR.1943-4774.0001493

785 Tang X., 2017. An improved method for predicting discharge of homogeneous compound channels
786 based on energy concept. Flow Measurement and Instrumentation Vol. 57(10), 57-63. DOI:
787 10.1016/j.flowmeasinst.2017.08.005

788 Tang X., 2019. Apparent shear stress-based method on an inclined interface plane for predicting
789 discharge in straight compound channels. MethodsX Vol. 6, 1323-1330. DOI:
790 10.1016/j.flowmeasinst.2019.01.012

791 Van Rooijen A., Lowe R., Ghisalberti M., Conde-Frias M. and Tan L., 2018. Predicting Current-
792 Induced Drag in Emergent and Submerged Aquatic Vegetation Canopies. Frontiers in Marine
793 Science Vol. 5(12), 449(1-14). DOI: 10.3389/fmars.2018.00449

794 Wang W.J., Huai W.X., Thompson S., Peng W.Q. and Katul G.K., 2018. Drag coefficient
795 estimation using flume experiments in shallow non-uniform. Ecological Indicators Vol. 92 (9), 367-
796 378. DOI: 10.1016/j.ecolind.2017.06.041

White B.L. and Nepf H.M., 2007. Shear instability and coherent structures in shallow flow adjacent to a porous layer. J. Fluid Mech. Vol. 593, 1-32. DOI: 10.1017/S0022112007008415

White B.L. and Nepf H.M., 2008. A vortex-based model of velocity and shear stress in a partially vegetated shallow channel. Water Resources Research Vol. 44(1), W01412(1-15). DOI: 10.1029/2006WR005651

Yang Z., Li d., Huai W. and Liu J.A., 2019. New method to estimate flow conveyance in a compound channel with vegetated floodplains based on energy balance. Journal of Hydrology Vol. 575(9), 921-929. DOI: 10.1016/j.jhydrol.2019.05.078

Zhang H., Wang Z., Xu W. and Wang H., 2019. Determination of emergent vegetation effects on Manning's coefficient of gradually varied flow. IEEE Access Vol. 7(10), 146778 - 146790. DOI: 10.1109/ACCESS.2019.2946917